Drug Delivery and Translational Research (2023) 13:1675–1698
https://doi.org/10.1007/s13346-022-01281-9

ORIGINAL ARTICLE

Liposome-polyethylenimine complexes for the effective delivery of HuR siRNA in the treatment of diabetic retinopathy

Shibani Supe[1] · Archana Upadhya[2] · Santosh Tripathi[4] · Vikas Dighe[3] · Kavita Singh[1]

Accepted: 7 December 2022 / Published online: 11 January 2023

Abstract

Diabetic retinopathy (DR) is a vision-impairing complication of diabetes, damaging the retinal microcirculatory system. Overexpression of VEGF (vascular endothelial growth factor) is implicated in the pathogenesis of DR. Human antigen R (HuR) is an RNA-binding protein that favorably regulates VEGF protein expression by binding to VEGF-encoding mRNA. Downregulating HuR via RNA interference strategies using small interfering RNAs (siRNAs) may constitute a novel therapeutic method for preventing VEGF protein overexpression in DR. Delivery of siRNAs to the cellular cytoplasm can be facilitated by cationic peptides or polymers and lipids. In this study, a cationic polymer (polyethylenimine (PEI)) and lipid nanoparticles (liposomes) were co-formulated with siRNA to form lipopolyplexes (LPPs) for the delivery of HuR siRNA. LPPs-siRNA were analyzed for size, zeta potential, serum stability, RNase stability, heparin stability, toxicity, and siRNA encapsulation efficiency. Cellular uptake, downregulation of the target HuR (mRNA and protein), and associated VEGF protein were used to demonstrate the biological efficacy of the LPPs-HuR siRNA, in vitro (human ARPE-19 cells), and in vivo (Wistar rats). In vivo efficacy study was performed by injecting LPPs-HuR siRNA formulations into the eye of streptozotocin (STZ)–induced diabetic rats after the development of retinopathy. Our findings demonstrated that high retinal HuR and VEGF levels observed in the eyes of untreated STZ rats were lowered after LPPs-HuR siRNA administration. Our observations indicate that intravitreal treatment with HuR siRNA is a promising option for DR using LPPs as delivery agents.

Keywords siRNA · HuR/ELAV · VEGF-A · Diabetic retinopathy · Lipopolyplexes · Polyethylenimine

Introduction

In recent reports by the International Diabetes Federation (IDF), the global population with diabetes mellitus was 463 million in 2019 and is expected to reach 700 million by 2045 [1]. Diabetic retinopathy (DR) is a common microvascular complication of diabetes and remains a leading cause of blindness if not timely addressed. All patients with type I diabetes, approximately 80% of insulin-dependent Type 2 diabetes and 50% with non-insulin-dependent type 2 diabetes, will have some retinopathy after 20 years of the disease [2]. If left untreated, DR progresses from mild, non-proliferative DR to moderate and severe non-proliferative DR before the occurrence of proliferative DR (PDR) and DME (diabetic macular edema) [3]. The PDR stage is due to ocular neovascularization that develops from the venous side of retinal circulation and may penetrate the inner limiting membrane into the vitreous. The nascent blood vessels that develop are delicate, leaky, and are eventually engulfed by fibrous connective tissue. This fibrous tissue can adhere to

Shibani Supe and Archana Upadhya joint first authors.

Dr. Kavita Singh is the first corresponding author and Dr. Vikas Dighe is the second corresponding author.

✉ Vikas Dighe
dighev@nirrh.res.in

✉ Kavita Singh
kspharma05@gmail.com; kavita.singh@nmims.edu

[1] Shobhaben Pratapbhai Patel School of Pharmacy and Technology Management, SVKM'S NMIMS, Mumbai, Maharashtra 400056, India

[2] Humera Khan College of Pharmacy, HK College Campus, Oshiwara, Jogeshwari (West), Mumbai, Maharashtra 400102, India

[3] National Centre for Preclinical Reproductive and Genetic Toxicology, ICMR-National Institute for Research in Reproductive and Child Health, J.M.Street, Parel, Mumbai, Maharashtra 400012, India

[4] Bombay Veterinary College, Sindhu Nagar, Parel Village, Parel, Mumbai, Maharashtra 400012, India

the surrounding collagenous tissue causing vitreous hemorrhage and/or retinal detachment on traction [2]. PDR can be further graded depending on the location of the vasculature, at the optic disc, or areas on the fundus (retina, iris, angle), and the presence or absence of vitreous hemorrhage [2, 4]. DME, characterized by edema, and disruption of retinal architecture, is defined as a retinal thickening or formation of hard exudates at or within 1 disc diameter of the macula center [5, 6].

PDR is associated with severe hypoxia leading to an overexpression of angiogenic factors (e.g., VEGF-vascular endothelial growth factor) compared to anti-angiogenic factors (e.g., PEDF-pigment epithelium-derived factor), a situation that favors the neovascularization [3]. VEGF is a crucial regulator of ocular angiogenesis and is implicated in DR and DME [7–9].

Strategies to inhibit the action of VEGF have been employed clinically for the treatment of DR, such as neutralizing anti-VEGF antibodies (Ranibizumab, off-label Bevacizumab), soluble VEGF decoy receptors (Aflibercept), VEGF-binding ligands (Pegatinib, a 28 nucleotide RNA aptamer that binds to the VEGF-A165 isomer) [4, 10, 11], and VEGF-downregulating nucleic acids. Bevasiranib (C and 5), a small interfering RNA (siRNA) against VEGF, has completed phase II clinical trials for the treatment of DME (NCT00306904).

The VEGF protein family includes members indicated as VEGF-A, VEGF-B, VEGF-D, VEGF-E, and PLGF (placental growth factor) [12]. VEGF-A is the major endothelial growth factor implicated in neovascularization and angiogenesis [13]. VEGF-A protein expression can be regulated transcriptionally and post-transcriptionally. Hypoxia is a trigger that upregulates the expression of VEGF-A. Hypoxia-inducible factor 1-alpha (HIF-α) mediates increased transcription of VEGF-A mRNA by binding to a hypoxia response element in the VEGF-A promoter region, causing the upregulation[13]. VEGF-A mRNA is stabilized post-transcriptionally in hypoxia by HuR (human antigen R or embryonic lethal vision (ELAV) protein [14–16]. HuR belongs to the family of expressed RNA-binding proteins (RBPs), which are involved in the pathogenesis of various disease conditions like cancer, chronic inflammation, and DR [17–19]. RBPs regulate mRNA transport, stability, and translation rates. HuR, one of the most studied RBPs, binds its target mRNAs through sequences rich in uridine or adenosine/uridine which are located in the non-coding regions of the transcript, in introns, or the 3′ untranslated regions (3′UTRs). Under normal conditions, HuR is present in the nucleus but shuttles to the cytoplasm to participate in mRNA processing under conditions of cellular stress, [20] to aid the cell's survival. HuR upregulates the expression of general stress response proteins and hypoxia response proteins, including HIF-1α and VEGF-A. Studies on the post-transcriptional regulation of VEGF have established that HuR stabilizes VEGF mRNA under hypoxic conditions by binding to a 40-bp RNA region in the 3′UTR [21]. HuR is thus a promising target for regulating VEGF-A protein expression. Amadio and colleagues, through their research, demonstrated that siRNA specifically targeting HuR when encapsulated in a lipoplex and injected into the eye of streptozotocin (STZ)–induced diabetic rats, drastically lowered VEGF and avoided diabetes-induced retinopathy [22].

Small interfering RNAs (siRNAs) are nucleic acid drugs that can downregulate target mRNA through RNA interference (RNAi) mechanisms [23]. The eye is an appealing organ for RNAi therapeutics since it is easily accessible, highly immune-privileged (due to restricted systemic exposure attributed to the existence of the blood-retina barrier (BRB)), and requires tiny, modest doses to exert a therapeutic impact [24, 25]. The eye, however, is a complex tissue and presents numerous barriers to nucleic acid delivery into its posterior segments (vitreous humor, inner limiting membrane (ILM), retina, inner blood-retinal barrier, retinal pigment epithelium) [25–27]. In the cellular cytoplasm, nucleic acid drugs are exposed to nucleases and cytoplasmic proteins, which encumber their functional efficacy.

Ocular delivery strategies of nucleic acids involve the use of viral and non-viral vectors [28–30]. Non-viral vectors for siRNA delivery can be based on cationic compounds such as liposomes/lipids or polymers, allowing for encapsulation or complexation of siRNAs in nano-sized particles [31, 32]. These cationic materials can form self-assembled complexes ("polyplexes" or "lipoplexes") based on the electrostatic attraction with negatively charged nucleic acids. The complexes protect the siRNA, reducing accessibility to nucleases and competitive ligands. Polyplexes generated from the cationic polymer such as polyethylenimine (PEI) show remarkable transport efficiency by enhancing the lysosomal protection and escape into the cytoplasm via osmotic rupture ("proton sponge effect"). However, they are associated with toxicity [33, 34]. Lipid-based carriers (liposomes) are also well established in nucleic acid delivery and show several advantages, including stability and favorable uptake mechanisms. However, protection of the siRNA payload from the lysosomal enzymes, its release from the endosomal/lysosomal compartment, and in vivo toxicity are major issues in liposome-based formulations [35, 36]. The favorable effects of both polymers and lipids may be enhanced when combined while reducing the toxic effects [37]. Interestingly, the latest evidence has shown that lipopolyplexes (LPPs) offer better biological characteristics for the transport of nucleic acid agents [38–40]. A study by Kwok and Hart observed the effectiveness of a branched form of PEI in forming stable complexes with siRNA [41]. LPP formulations containing branched 25 kDa PEI as a core material in combination with multivalent cationic lipids (DOCSPER, DOSPER) [42–44],

or PEI/DNA complexes coated with a combination of cationic or anionic and neutral lipids cholesterol and PEG lipids [38], are promising reagents for transfection or in vivo DNA delivery [45]. In this study, we have evaluated the efficiency of HuR siRNA encapsulated in DPPC-PEI-based LPP, in suppressing HuR expression and their effects on VEGF protein levels in vivo and in vitro compared to their parent polyplex.

Materials and methods

Materials

siRNA targeted to human HuR mRNA was designed using BLOCK-iT™ RNAi Designer, ThermoFisher software, and procured from Merck, India. MISSION® siRNA Fluorescent Universal Negative Control #1, 6-FAM-siRNA (6-Carboxyflourescein-siRNA), MISSION® siRNA Universal Negative Control #1 (Sc siRNA), and branched polyethylenimine (average molecular weight (MW) 25 K) were purchased from Merck, India. The 1,2-dipalmitoyl-sn-glycero-3-phosphocholine (DPPC), hydrogenated soya phosphocholine (HSPC), and methoxy polyethylene glycol 2000–1,2-distearoyl-sn-glycero-3- phosphoethanolamine (mPEG2000–DSPE) were obtained as gift samples from the Lipoid Ltd., Ludwigshafen, Germany. Dioleoyl-sn-glycero-3-phosphoethanolamine (DOPE) was purchased from Avanti Polar Lipids (Alabaster, AL). ARPE-19 (human retinal pigment epithelial cells) was a kind gift from Dr. Debashish Das, Narayana Nethralaya Foundation, Bangalore, India. Cell culture reagents DMEM F12 (Dulbecco's Modification of Eagle's Medium), fetal bovine serum (FBS), Dulbecco's phosphate-buffered saline (DPBS), antibiotic solution (penicillin G, streptomycin, and amphotericin B solution), L-glutamine, and 3-(4,5-dimethylthiazol-2-ly)-2,5-diphenyl-tetrazolium bromide (MTT) were purchased from Himedia (Mumbai, India). Lipofectamine 2000, SuperScript™ IV First-Strand synthesis system, Opti-MEM, and TRIzol™ RNA isolation reagent were purchased by ThermoFisher Scientific (MA, USA). All other chemicals used in the study were of analytical grade and were purchased from local vendors in Mumbai, India. The source of heparin was Heparin injection IP (FLAGORIN-5000™).

siRNA sequences

siRNA sequence targeting human HuR mRNA was designed using BLOCK-iT™ RNAi Designer, ThermoFisher, and siRNA sequence targeting rat HuR mRNA was obtained from the literature [22]. The sequences, human HuR siRNA and rat HuR siRNA, were analyzed by the NCBI nucleotide BLAST algorithm to check for specificity and were found to have insignificant off-target hits in the human and rat nucleotide databases, respectively. The sequences of both siRNAs (human and rat) are given in Table 1.

Optimization of PEI: siRNA complexes

Complexation of the siRNA to PEI was assessed by gel retardation assay. Complexation of positively charged PEI with siRNA will retard the siRNA movement on agarose gel electrophoresis towards the positive electrode. This indicates the reduction or neutralization of the negative charge on the nucleic acid due to interaction with the polymer. Briefly, branched PEI (MW~25 K) at different N/P ratios (ratio of amine groups of PEI to the phosphate groups of siRNA) were incubated with siRNA (20 pmol) to evaluate its complexation ability. As a positive control for maximum migration within the gel, 20 pmol of naked siRNA was used. All complexes were analyzed on 2.5% w/v agarose gel containing 0.5 µg/mL of ethidium bromide. Gel electrophoresis was carried out for 45 min at 70 V in 1X TAE (Tris–acetate-EDTA) buffer diluted from the 50X TAE buffer from ThermoFisher scientific buffer (pH 8.4) with autoclaved 1% DEPC (diethyl pyrocarbonate, Sigma-Aldrich) treated distilled water. The nucleic acid bands on the gel were visualized under ultraviolet light, and the image was captured using the Alphaimager HP gel doc system (Cell Biosciences, CA). The optimum concentration of PEI was fixed after the assessment. The optimum ratio of PEI:siRNA was found to be at a N/P ratio of 20.

Preparation of lipopolyplexes-siRNA (LPPs-siRNA)

Branched PEI was added to 20 pmol of siRNA to obtain a N/P ratio of 20, followed by gentle pipetting and incubation at 37 °C for 30 min. Liposome-1, DPPC/HSPC/cholesterol/mPEG2000-DSPE (10:33:26:6 on molar basis), and liposome-2, DPPC/DOPE/HSPC/cholesterol/mPEG 2000-DSPE

Table 1 siRNA sequences. Sequences used in the in vitro human cell line study and in vivo rat study.

Sr. no.	Species	Strand	Sequence
1.	Human	Sense strand	5′-GUUUAUCCGGUUUGACAAA[dT][dT]-3′
		Anti-sense strand	5′- UUUGUCAAACCGGAUAAAC[dT][dT]- 3′
2.	Rat	Sense strand	5′-GCUUGAGGCUUCAGUCCAATT[dT][dT]-3′
		Anti-sense strand	5′-UUGGACUGAAGCCUCAAGCCG[dT][dT]-3′

(10:5:33:26:6 on molar basis) were prepared by thin-film hydration method. Lipids were dissolved in chloroform in a 50-mL round bottom flask at the given molar ratios. Chloroform was evaporated in a rotary flask evaporator (IKA, HB-10, USA) under vacuum and 40 °C temperature, 100 rpm speed, to produce a thin film of lipids. Nitrogen was purged gently to remove any remaining traces of chloroform. The thin lipid film obtained was hydrated with autoclaved 1% DEPC-treated distilled water at 55 °C for 1 h, followed by sonication in an ultrasound bath sonicator for a few minutes at the same temperature. The suspension was finally extruded 11 times through a 200-nm polycarbonate membrane (Avanti Polar Lipids) in a Mini-Extruder at 45 °C to form unilamellar liposomes. Lipopolyplexes (LPPs) were prepared by mixing and vortexing the liposomes with PEI-siRNA polyplexes in a mass ratio of 7:1. The formed ternary complexes were then incubated for at least 1 h at 37 °C and analyzed by gel retardation assay techniques to assess the complexation, stability to heparin, serum, and RNase [40, 46]. Ethidium bromide intercalation assay was used to estimate the encapsulation efficiency and stability of siRNA within complexes in the presence of a competitive ligand (heparin). Lipopolyplexes with DPPC/HSPC/cholesterol/mPEG 2000-DSPE are designated as LPP_1 and lipopolyplexes DPPC/DOPE/HSPC/cholesterol/mPEG 2000-DSPE are designated as LPP_2 in this manuscript.

Characterization of LPPs-siRNA

Gel retardation assay techniques

Complexation of the siRNA to PEI and the subsequently formed LPPs were assessed by gel retardation assay techniques.

Polyanion competition assay The stability of complexes (polyplexes and lipopolyplexes) with siRNA (20 pmol) was evaluated by measuring siRNA release from complexes in the presence of competing polyanion heparin. Polyplexes (PEI-siRNA (20 pmol)) and LPPs (lipidated PEI-siRNA (20 pmol)) were prepared and treated with different quantities of heparin from 0.25 IU to 2 IU for over 30 min. After 30 min of incubation with heparin, all these samples were analyzed on 2.5% w/v agarose gel containing ethidium bromide and run in an electrophoresis chamber containing 1X TAE (buffer made in nuclease-free DEPC-treated water) at 70 V for 45 min.

Serum stability assay The assay was performed as per the protocol given in the paper by Khatri and colleagues [47, 48] but with some modifications. Briefly, naked siRNA (100 pmol) and LPPs containing 100 pmol siRNA were incubated with 10 µL of FBS and the final volume of the reaction mixture was 100µL. All samples were incubated at 37 °C for 4 h. After incubation, 50µL of TRIzol™ was added to all samples. The samples were centrifuged at 12,000 g for 15 min at 4 ℃, and the upper aqueous layer (20µL) was extracted into an Eppendorf to which 3µL of a 6X DNA loading buffer (ThermoFisher Scientific) was added and run-on horizontal gel electrophoresis apparatus at conditions described above. The propensity of the lipopolyplexes to protect the siRNA in the presence (+) and absence (−) of serum was assessed.

RNase A protection assays LPPs-siRNA (20 pmol siRNA) were incubated with RNase A (10U/mL, GeNei™) at 1U/µg of siRNA at 37 °C for 30 min. The reaction was terminated by 0.5 µL of RNase OUT (100 mM, ThermoFisher Scientific), and LPPs were disassembled by Triton X-100 and 10 IU of heparin. The samples were kept at room temperature for 15 min and analyzed on gel electrophoresis for the siRNA band integrity under the above-mentioned conditions.

Ethidium bromide (EtBr) intercalation assays

Measurement of siRNA encapsulation efficiency of lipopolyplexes Ethidium bromide intercalation assay was used to assess the efficacy of the lipopolyplexes in encapsulating siRNA (20 pmol) and to measure the unbound/uncomplexed siRNA. Furthermore, the propensity of the lipopolyplexes to retain the siRNA in the presence of a competitive ligand, heparin, was also evaluated. EtBr tends to fluoresce on intercalation with siRNA; thus, an increase in fluorescence indicates the presence of uncomplexed/unbound/released siRNA. The plain formulation components (i.e., without siRNA) were found to give negligible fluorescence with EtBr compared to EtBr alone and were not considered in the calculations [49].

$$\%\ \text{Encapsulation efficiency} = 100 - \%\text{Relative Fl.}$$

$$\%\ \text{Relative Fl} = [(\text{Fl.(obs)} - \text{Fl.(EtBr)})/(\text{Fl.(siRNA} + \text{EtBr}) - \text{Fl.(EtBr)})] * 100$$

where Fl. (obs)—fluorescence of complexed siRNA + ethidium bromide

Fl. (EtBr)	fluorescence of ethidium bromide alone
Fl. (siRNA + EtBr)	fluorescence of uncomplexed siRNA + ethidium bromide

siRNA release in the presence of competitive ligand (heparin) The LPPs formed with 20 pmol of siRNA were exposed to 0.25–2 International Units (IU) of heparin for 30 min at 37 °C. After 30 min of heparin treatment, samples were placed in a 96-well plate (Microplates for Fluorescence-based Assays, Nunc™), and 50µL of 0.4 µg/mL of ethidium bromide was added. The plate was then incubated in the dark for 30 min at 37 ℃. Finally, the fluorescence at the excitation and emission wavelengths of 510 and 590 nm were determined by the SpectraMax iD3 multimode microplate reader (Molecular Devices, USA). The relative fluorescence was calculated using the following equation:

$$\% \text{ Relative Fl} = 100 * [(\text{Fl.(obs)} \pm \text{heparin} - \text{Fl.(EtBr)}) / (\text{Fl.(siRNA} + \text{EtBr)} - \text{Fl.(EtBr)})]$$

$\text{Fl(obs)}_{\pm\text{heparin}}$	fluorescence of complexed siRNA + ethidium bromide ± heparin
Fl. (EtBr)	fluorescence of ethidium bromide alone
Fl. (siRNA + EtBr)	fluorescence of uncomplexed siRNA + ethidium bromid

Measurement of complex sizes and zeta potentials

The average particle size and zeta potential of polyplex-siRNA (100 pmol), liposomes, and LPPs-siRNA (100 pmol) were analyzed by differential light scattering (DLS) with a Malvern Zetasizer Nano ZS-90 (Malvern Instruments, Malvern, UK). Before analysis, the complexes were diluted 100-fold with autoclaved 1% DEPC-treated distilled water and evaluated at room temperature of 25 °C. Analysis was repeated three times, and the mean value was recorded.

Transmission electron microscopy (TEM)

Suspensions of PEI-siRNA (100 pmol) polyplexes and LPPs-siRNA (100 pmol) were individually placed on Formvar/carbon grids (Plano, Wetzlar, Germany) and incubated for 10 min. The excess liquid was drained, and the grid was air-dried, followed by negative staining with a 2% phosphotungstic acid hydrate solution (pH 7.0). The imaging was conducted at 300 kV using the TEM (TECNAI 12 BT/FEI) equipped with a retractable high-resolution slow-scan CCD-Camera (GATAN Inc. USA).

Scanning electron microscopy

LPPs-siRNA (100 pmol) suspensions were spotted on an aluminum grid and dried in a vacuum. The samples were analyzed using the scanning electron microscope equipped with a field emission, a JEOL JSM 6380, after sputtering the sample with platinum using a coater JEOL JSM 1600 and imaged with SEM (JEOL JSM-6510, Tokyo, Japan).

ARPE-19 cell culture

Human ARPE-19 cells were cultured in a 1:1 mixture of Dulbecco's modified Eagle's medium F12 with 2.5 mM L-glutamine, 29.03 mM sodium bicarbonate, 0.5 mM sodium pyruvate, and 10% fetal bovine serum. The cells were maintained at 37 °C in a humidified atmosphere with 5% CO_2. Cells at passages 18–28 were used in all the experiments, and seeding cells were counted in a hemocytometer with trypan blue staining.

In vitro cellular toxicity assays

Hemolysis study with rat RBCs

Hemolysis assay was performed by using the method described in Upadhya and Sangave [50] with minor modifications. The hemolytic propensity of LPPs and their parent polyplexes was evaluated using an in vitro erythrocyte lysis test at siRNA doses ranging from 10 to 100 pmol. Blood (< 0.5 mL) was taken from Wistar rats via a retro-orbital puncture in tubes (Vacutainer® Heparin Tubes) and centrifuged at 1200 g for 10 min at 4 °C to sediment red blood cells (RBCs). The RBC pellet was washed with phosphate-buffered saline (PBS-0.144 g/l KH_2PO_4, 9.0 g/l NaCl, 0.726 g/l Na_2HPO_4 pH7.4) 3–4 times to remove plasma from proteins and resuspended in the PBS. The suspended RBCs were counted using a blood cell count analyzer (Sysmex-Poch-100i, TransAsia). The cell suspensions were diluted to a concentration of 10^8 cells/mL in HEPES (4-(2-hydroxyethyl)-1-piperazineethanesulfonic acid) buffered glucose (HBG). Negative and positive controls were plain RBC suspension in HBG and 1% Triton X-100 in HBG, respectively. The formulations were incubated for 4 h at 37 °C and analyzed for heme released in the supernatant at 540 nm using the UV–visible spectrophotometer (Perkin Elmer). The equation used to determine the percentage of hemolysis:

$$\% \text{ hemolysis} = (\text{Abs.sample}/\text{Abs.PC}) \times 100$$

where Abs.sample and Abs.PC area absorbance values at 540 nm of the individual sample and the positive control, respectively.

MTT assay with ARPE-19 cells

In vitro cytotoxicity of the LPPs and their parent polyplexes were determined by MTT assay using ARPE-19 cells. ARPE-19 cells at a density of 7000 cells/well were seeded on a 96-well plate and incubated for 24 h at 37 °C in humidified air with 5% CO_2. Cells were then incubated separately with LPP_1-siRNA, LPP_2-siRNA, and PEI-siRNA complexes at varying siRNA concentrations (1 pmol-10 pmol of siRNA) for 4 and 24 h. After treatment, the media was removed, and 200 µL of 0.2 mg/mL MTT (3-(4,5-dimethylthiazol-2-yl)-2,5-diphenyl-tetrazolium bromide, Merck) solution in DPBS (Dulbecco's phosphate-buffered saline) was added and incubated for 4 h. At the end of the incubation period, the MTT solution was removed from the wells, followed by the addition of 100 µL of dimethyl sulfoxide. Cell viability in each well was assessed using an enzyme-linked immunosorbent assay plate reader (Bio-Rad, USA) to identify formazan products produced by live cells by reducing MTT. The absorbance was measured at 570 nm and 650 nm. The DPBS-treated cells (untreated cells) were considered a negative control. Cell viability for each formulation treatment was normalized to the value obtained from the negative control. The cell viability was calculated by using the following equation:

$$\begin{aligned}\%\ \text{cell viability} = 100 * [&(\text{Abs. treated cells (570 nm)} \\ &- \text{Abs. treated cells (650 nm)}) \\ &/(\text{Abs. of untreated cells (570 nm)} \\ &- \text{Abs. of untreated cells (650 nm)})]\end{aligned}$$

In vitro cell uptake study

Flow cytometry

The protocol was a modification of previous methods [51, 52]. Briefly, ARPE-19 cells were seeded in six-well plates with Dulbecco's modified Eagle's media at a density of 5×10^5 cells per well and cultured for 24 h to attain 75% confluence. The culture medium was withdrawn after 24 h, and the cells were rinsed with DPBS solution before adding polyplexes and LPPs, loaded with 100 pmol 6-FAM-siRNA in 1 mL of serum-free culture medium. After 4 h, the cells were harvested by trypsinization (0.05% trypsin and 0.02% EDTA solution) and suspended in DPBS at approx. 1×10^6 cells/mL for flow cytometric analysis. Fluorescence activity was used to assess cell integrity using a fluorescence-activated cell sorter (FACS-BD-Aria III, BD, USA). Values obtained were compared with that observed with naked 6-FAM-siRNA and 6-FAM-siRNA complexed with Lipofectamine 2000.

Confocal laser scanning microscopy

ARPE-19 cells were seeded at a density of 10,000 cells well in six-well plates containing a flame sterilized glass coverslip ($0.17mm^2$) at the well-bottom. After 24 h, cells were transfected with polyplexes and LPPs loaded with 6-FAM-siRNA (100 pmol) for 4 h in a serum-free medium. After 4 h of incubation, cells were rinsed with cold DPBS immediately and fixed with a chilled 4% w/v paraformaldehyde solution for 10 min, followed by three washes with chilled DPBS. Cells were stained for 10 min with cell nuclei dye (DAPI), and then washed three times with DPBS to remove excess DAPI (4′,6′-diamidino-2-phenylindole). After three DPBS washes, coverslips were mounted on slides with a confocal laser scanning microscope for confocal microscopy. (LSM 710, Carl-Zeiss Inc., USA). The observations were compared with naked Fam-siRNA and Fam-siRNA complexed with Lipofectamine 2000.

Gene downregulation studies in ARPE-19

For the in vitro gene downregulation study, ARPE-19 cells were seeded onto 6 well plates with a density of 7.5×10^5 cells/well. PEI-HuR siRNA polyplexes and LPP_2-HuR siRNA were added to the respective cells at 80% cell confluency. Three different doses of siRNA in the complexes were used, i.e., 50 pmol, 100 pmol, and 150 pmol. Commercially available transfecting agent Lipofectamine 2000 was also complexed with equivalent amounts of siRNA and used for comparison purposes, with transfection carried out according to the manufacturer's (ThermoFisher) instructions. To remove bias due to the off-targeting effects of siRNA, LPPs and Lipofectamine 2000 were also loaded with equivalent doses of scrambled siRNA, and the values obtained were considered in the evaluation. Gene downregulation was evaluated by real-time PCR and western blotting techniques. All transfection experiments were carried out in triplicates, each repeated twice; the results represent the averages of these experiments.

Real-time polymerase chain reaction (RT-PCR)

siRNA-mediated downregulation of HuR was quantified by knockdown of HuR mRNA by using real-time PCR (RT-PCR) technique. After 48 h of transfection, total RNA was isolated from ARPE-19 cells using TRIzol™ reagent (Invitrogen), and cDNA was synthesized by using SuperScript™ IV reverse transcriptase (Invitrogen) following the vendor's protocol. Primers used in the PCR were designed by using Oligo Explorer™ 1.2 software. Sequences of the Human HuR primers and glyceraldehyde 3-phosphate dehydrogenase (GADPH) primers are given in Table 2. The primer sequences were screened using the NCBI nucleotide BLAST

Table 2 Primer sequences. Primer sequences used for the real-time PCR of ARPE-19 cells and rat retinal tissue

Sr. no.	Species	Gene	Direction	Oligonucleotide sequence (5′→3′)
1.	Human	HuR	Forward	ATAAAGTAGCAGGACACAGC
			Reverse	AGCATACGACACCTTAATGG
2.		GAPDH	Forward	CATCACCATCTTCCAGGAGC
			Reverse	GCAGAGATGATGACCCTTTTGG
3.	Rat	HuR	Forward	GGGATAAAGTTGCAGGACACAG
			Reverse	GATAACCTCTGAGCTTGGGC
4.		GAPDH	Forward	TCGGTGTGAACGGATTTGGC
			Reverse	TTGAACTTGCCGTGGGTAGA

search to confirm their specificity (https://blast.ncbi.nlm.nih.gov/Blast.cgi). RT-PCR was performed using Power SYBR Green Mastermix (Applied Biosystems, Warrington, UK). Reactions were analyzed upon an ABI 7500 real-time PCR machine using the following cycle conditions: 50 °C for 2 min, 95 °C for 2 min, followed by 40 cycles at 57 °C for 15 s, 72 °C for 1 min, and 60 °C for 1 min. Results were normalized against GAPDH expression. The cDNA transcript levels were determined according to the $2^{-\Delta\Delta Ct}$ method since the PCR efficiencies for both genes (HuR and GAPDH) were comparable.

HuR and VEGF protein levels in ARPE-19 cells

The effect of downregulation of HuR mRNA on HuR and VEGF protein was evaluated by western blot and ELISA assay, respectively. After 48 h of a 4-h transfection with polyplexes-HuR siRNA, lipopolyplexes-HuR siRNA, and Lipofectamine 2000-HuR siRNA, proteins were isolated from respective cells by RIPA Lysis and Extraction Buffer (Catalog number-89900; Thermo Scientific) containing protease inhibitors (ROCHE cOmplete™ Protease Inhibitor Cocktail, Thermo Scientific) (1:100) and quantified with Bradford reagent (Thermo Scientific) according to manufacturer's protocol using bovine serum albumin protein as a standard. Standard SDS-PAGE (sodium dodecyl sulfate–polyacrylamide gel electrophoresis) Laemmli system was used to separate the proteins in the extracts. Each lane of the PAGE was loaded with 100 µg of protein. Subsequently, the resolved proteins on the gel were transferred onto nitrocellulose membranes and analyzed by western blotting techniques (Bio-Rad). Skim milk powder (5%) in TBST (20 mM Tris–HCl, 150 mM NaCl, 0.2% Tween 20, pH 7.4) was used as a blocking solution for all membranes for 1 h at room temperature followed by incubation with HuR (1:500) antibody ((ab200342) from rabbit), or β-actin (1:200) antibody ((ab8227) from rabbit) (Abcam, UK) as a control overnight at 4 ℃. This is followed by culturing with the goat anti-rabbit secondary antibody (ab6721) (1:5000, Abcam, UK) for 1 h. The blotting images were taken by a Gel Doc imaging system (Bio-Rad, India) using an Amersham Biosciences ECL kit for band recognition.

VEGF-A protein levels in the extracts were quantified by a Quantikine human VEGF ELISA (Enzyme-Linked Immunosorbent Assay) kit (DVE00; R&D Systems, Minneapolis, MN, USA). The results are expressed as VEGF per mg of total protein [53].

Animal experiments

Male Wistar rats were kept in cages maintained at a controlled temperature (25 ± 1 °C) and humid atmosphere (relative humidity (45 − 55%)), with a 12-h light/dark cycle. The animals were fed on house-prepared standard rat chow pellets (soy-free) and water ad libitum. The experiments were conducted as per the guidelines of the Committee for the Purpose of Control and Supervision of Experiments on Animals (CPCSEA), India. The study protocol was approved by the Institutional Animal Ethics Committee (IAEC) [Application numbers: NIRRH/IAEC/ 20/20]. The intraperitoneal injection of Streptozotocin (STZ) (STZ, Sigma-Aldrich, Bangalore, India) at a dose of 55 mg/kg, suspended in cold, sterile citrate buffer (0.1 M, pH 4.5), was used to cause diabetes [22, 54]. STZ leads to the destruction of pancreatic island β cells in rodents. After 72 h of STZ injection, plasma blood glucose levels were measured to confirm diabetes induction. Animals with random blood glucose levels greater than 250 mg/dl were classified as diabetic and recruited for the study. Animals in the control group (CTR) received only citrate buffer. Twenty-five days post diabetes induction, after the development of retinopathy (on Fundoscopic examination), PEI-polyplexes, and LPP_2 loaded with rat HuR siRNA (2.5 pmol/µL or 2.5 µM) (2 µL in RNAse-free water; Thermo Scientific) were administered through the intraocular route (all intraocular administrations were through the intravitreal route). Triamcinolone acetate (TRIM), used to treat retinopathy therapeutically [55], was administered intraocularly in a single dose. The formulation of KENACORT®, Abbott (TRIM 40 mg/mL), was used as a source of TRIM and was administered in a volume of 1.4 µL as a therapeutic control [55]. TRIM is

an intermediate-acting corticosteroid suspension that has shown remarkable efficacy in treating advanced DR [56]. Before the intravitreal injections, Tropicamide eye drops (Sunways India Pvt Ltd.) and topical anesthetic (5 g/L tetracaine hydrochloride, Santen, Japan) was administered until the pupils of the rats were dilated. The rats were anesthetized with ketamine hydrochloride, 80 mg/kg BW(body weight) i.p (intraperitoneal); xylazine, 10 mg/kg BW i.p., following which 2 µL of complexes containing rat siRNA (5 pmol) was injected intravitreally, into the right eye of rats using a 1-mL Hamilton syringe. The microsyringe needle was introduced 0.5 mm posterior to the corneoscleral limbus into the vitreous cavity of the right eye in the siRNA group, avoiding the crystalline lens, with the aid of a surgical microscope. After the intravitreal injection, ofloxacin eye ointment (Exocin Eye Ointmen™, Allergan) was applied to the eyes to avoid infection. All fellow eyes were injected with control injection (2µL of sterile PBS). The animal's disease control (STZ/DC) was grouped according to the formulation of siRNA complexes and were categorized as (1) PEI-HuR siRNA, (2) LPP_2-HuR siRNA, and (3) TRIM (4) untreated DC. A disease-free control group (not treated with STZ) was also maintained for comparison purposes. All the animals were sacrificed 48 h after siRNA injection. The final group sizes for all measurements were $n = 8$. Euthanasia was performed with CO_2 inhalation after 48 h, and the retinal tissue was collected [57]. Retinal tissue was divided for RNA and protein extraction. For RNA extraction, retinal tissue was homogenized in TRIzol™ at 4℃ using the homogenizer (Polytron PT 2500E, Kinematica, Switzerland) according to the manufacturer's instructions. The isolated RNA was reverse transcribed to cDNA using the SuperScript IV kit (ThermoFischer) HuR gene downregulation was estimated by real-time PCR techniques. Protein extraction was carried out by homogenizing retinal tissues in RIPA buffer containing protease inhibitors (ROCHE cOmplete™ Protease Inhibitor Cocktail, Thermo Scientific) (1:100), followed by protein estimation. HuR protein expression was analyzed by using western blot techniques and VEGF protein levels were further estimated using Rat Vascular Endothelial Growth Factor (VEGF) ELISA (KINESIS Dx, Krishgen Biosystems, India). Fundoscopic observations by indirect ophthalmoscopy (Omega 500 Binocular Indirect Ophthalmoscopy, Heine Optotechnik, Gilching, Germany) were done before the intravitreal injections and at the time of sacrifice. In addition, a 90 D lens (a component of the ophthalmoscope) was used for the fundus examinations (Wlch Allyn, Skaneateles Falls, NY, USA).

Retinal histology

The retinal histology was performed to evaluate the morphological changes in the rat retina with DR before and after the siRNA treatment. Eyes were enucleated and fixed overnight with Davidson's fixative (40% v/v formaldehyde, 30% v/v ethanol, 5% v/v glacial acetic acid) and then stored in 0.1 M sodium phosphate (pH 7.6) containing 4% w/v paraformaldehyde. The paraffin-embedded retinal Sects. (4 mm thickness) were taken using a microtome (Leica Biosystems, Germany). Retinal tissue was stained using Mayers Hematoxylin–Eosin (HE stain) and the thickness of the stained area was observed. Slides were observed under an optical microscope (Nikon Fx-35A, Japan).

Statistical analysis

The mean of at least three observations is used to calculate all values, which are expressed as mean ± SEM unless otherwise stated. One-way or two-way ANOVA with Dunnett's test or Bonferroni was used for statistical analysis, with $p < 0.05$ being the threshold for statistical significance.

Results

Evaluation of LPPs by agarose gel electrophoretic techniques

As described in the "Materials and methods" section, LPP was made by non-covalent complexation of PEI-siRNA with liposomes by incubating PEI-siRNA polyplexes with prepared liposomes without chemical coupling. A gel retardation assay was carried out to evaluate the complexation of siRNA with PEI and within the LPP. The loss in the mobility of siRNA indicated that PEI in an N/P ratio of 20:1 could condense siRNA effectively (Fig. 1A). This ratio of PEI to siRNA was used for liposomal interaction and preparation of LPPs. The ternary complexation of siRNA in the LPPs was successful as determined by the assay.

Serum stability assay

LPP_1 and LPP_2 were evaluated for their ability to shield the encapsulated siRNA on exposure to serum. The LPPs-siRNA were exposed to serum for 4 h, following which the siRNA was extracted by TRIzol™ and subjected to agarose gel electrophoresis. Agarose gel electrophoresis was used to assess the siRNA band integrity after exposure to serum and RNase. Figure 1B shows that LPP_1-siRNA and LPP_2-siRNA with (+) and without (−) serum treatment reflected similar siRNA band intensities as the untreated (naked) siRNA (used as positive control).

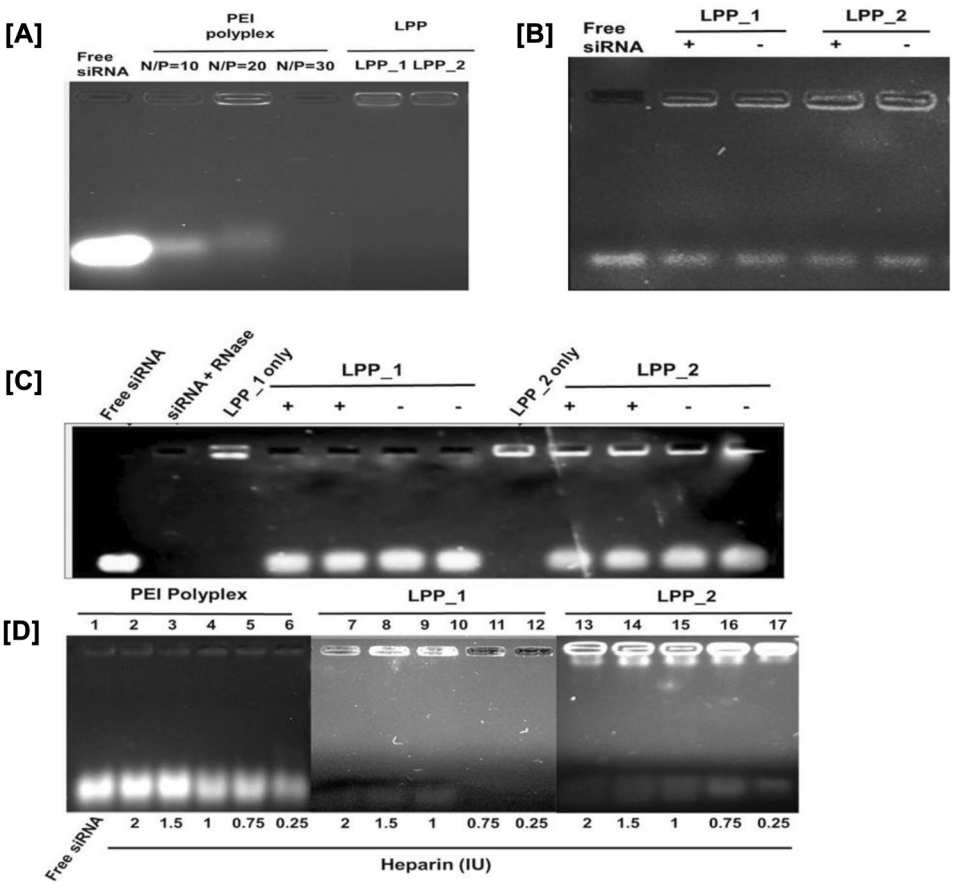

Fig. 1 **A** Gel retardation assay of polyplexes and lipopolyplexes. The polyplexes at an N/P ratio of 20 and above could complex siRNA. The lipopolyplexes (LPP_1 and LPP_2) also demonstrated the complete complexation of siRNA. **B** Serum stability assay. The LPPs could shield the siRNA from the serum proteins and nucleases indicated by similar siRNA band intensities in the (+) treated and (−) untreated samples. **C** RNase stability assay. The LPPs could shield the siRNA from RNaseA indicated by similar siRNA band intensities in the (+) treated and (−) untreated samples. The treated uncomplexed siRNA was completely degraded by the RNase. **D** Heparin competition assay. All complexes were exposed to heparin in the range of 0.25–2 IU and analyzed for the siRNA displacement by agarose gel electrophoresis

RNAse protection assay

The LPPs were evaluated for their capability to protect the encapsulated siRNA in the presence of RNA degrading enzymes such as RNase A. The complexes were exposed to 30 min of RNase A, after which an RNAse inhibitor was added, and the complexes were undone using a surfactant (Triton X-100) and a competitive ligand (heparin). The integrity of the siRNA was evaluated by agarose gel electrophoresis. Both LPP_1 and LPP_2 could protect the siRNA from RNase A (Fig. 1C). As seen in the figure, the bands of siRNA were sharp and comparable to that obtained by the positive control (untreated naked siRNA). The RNAse could completely degrade the uncomplexed (naked siRNA) used as a negative control.

Heparin competition assay

The stability of the ternary complexes was analyzed in the presence of polyanion heparin. As shown in Fig. 1, siRNA was released from the PEI polyplex in the presence of 0.25 IU of heparin. Lipidation of siRNA polyplexes with liposome-1 and liposome-2 was found to hinder the displacement of siRNA by heparin. It has been found that LPP_2 could significantly retain siRNA in the presence of 2 IU of heparin (indicated by the bright bands observed in the well suggesting retention of siRNA) while LPP_1 partially released siRNA when exposed to ≥ 1 IU of heparin.

Ethidium bromide intercalation assays

Measurement of siRNA encapsulation efficiency

The binding efficiency of the lipidated and unlipidated PEI-siRNA complexes with siRNA was determined by using an ethidium bromide intercalation assay. The % relative fluorescence indicates the percentage of free siRNA bound with ethidium bromide after subtracting the background fluorescence of EtBr and multiplying by 100. It has been observed that PEI at N/P = 20 showed 76.51 ± 0.13% siRNA encapsulation ability while LPP_1 showed 90.94 ± 0.25% and LPP_2 showed 96.03 ± 0.49% encapsulation ability of siRNA as shown in the Fig. 2A. Lipidation of PEI-siRNA polyplexes increases the complexation efficiency.

Measurement of siRNA release in the presence of competitive ligand (heparin)

The release of siRNA in the presence of heparin was also confirmed by the EtBr intercalation assay. In Fig. 2B, it

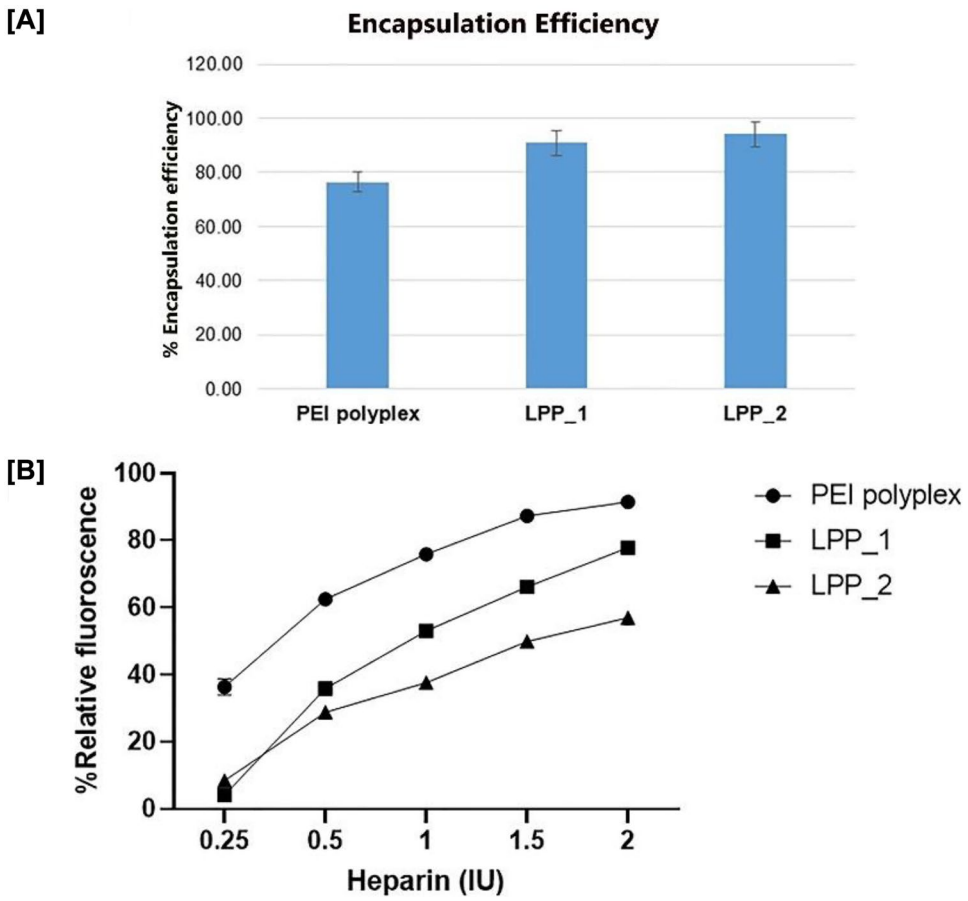

Fig. 2 **A** Encapsulation efficiency of siRNA in polyplex and LPPs (LPP_1-siRNA and LPP_2-siRNA) and **B** siRNA release from all the complexes in the presence of different concentrations of heparin was determined using an ethidium bromide intercalation assay (***$p < 0.0001$). Results are represented as mean ± SD ($n = 3$)

has been observed that more than 85% of the siRNA was released from the PEI-siRNA polyplex at 2 IU of heparin. LPP_1 released ~80% of siRNA at 2 IU of heparin, while LPP_2 released ~50% of the encapsulated siRNA. Thus, LPP_2 showed better stability in the presence of the siRNA competitive polyanion. i.e., heparin.

Measurement of complex sizes and zeta potentials

The size, the polydispersity index (PDI), and the surface charge of the polyplexes liposomes and LPPs were measured, and the values are tabulated in Table 3. Both the LPPs present a Z-average diameter of around 200–250 nm with PDI lower than 0.35.

Electron microscopy analysis

The structure of these LPPs was determined using SEM micrographs. Micrographs of both the LPPs, shown in Fig. 3A1 and A2, displayed relatively spherical-shaped particles of size ranging from 200 to 280 nm, confirming the observations in the DLS analysis.

Table 3 Effect of lipidation of PEI-siRNA polyplex on particle size and zeta potential of polyplex

Formulation	Particle size (nm)	PDI	Zeta potential (mV)
PEI-siRNA polyplex	207.25 ± 55.24	0.114 ± 0.14	+10.19 ± 2.39
Liposome 1	121.14 ± 55.24	0.2 ± 0.24	−8.35 ± 3.18
LPP_1 (ternary complex of liposome 1 and PEI-siRNA)	238.22 ± 9.17	0.329 ± 0.08	+5.21 ± 2.08
Liposome 2	180.32 ± 10.05	0.254 ± 0.27	−7.31 ± 5.17
LPP_2 (ternary complex of liposome 2 and PEI-siRNA)	250.05 ± 10.22	0.311 ± 0.12	+7.88 ± 1.32

The values are averages of three measurements ± standard deviations (SD)

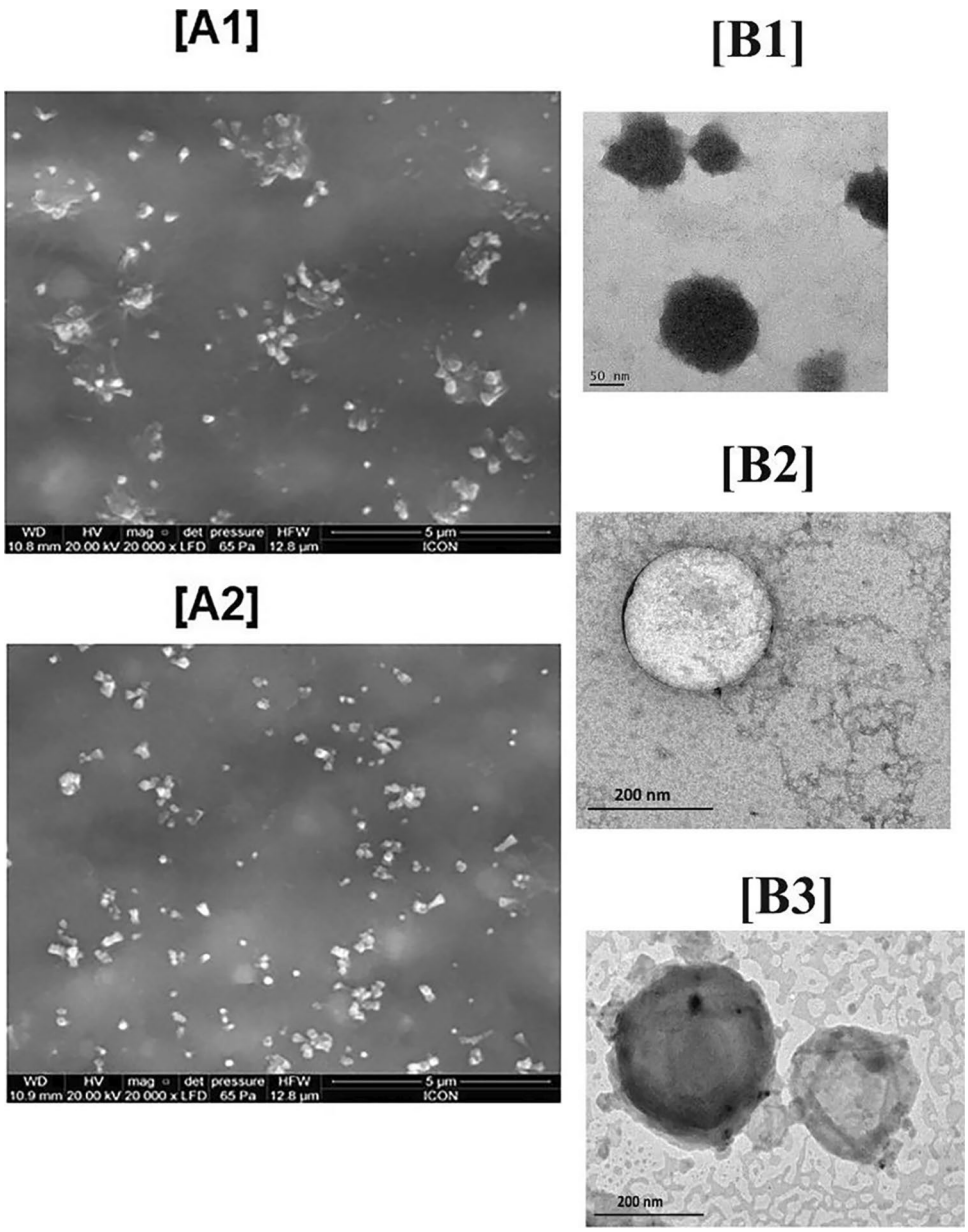

Fig. 3 SEM and TEM images. Panel **A** A1 and A2 shows the SEM images of LPPs, LPP_1 and LPP_2 respectively (scale bar 5 µm). Panel **B** B1, B2, and B3 are representative TEM images of PEI-siRNA polyplex, liposome (liposome 2) and lipopolyplex respectively

For TEM analysis, siRNA, liposomes, and lipopolyplexes were stained with phosphotungstic acid for visualization (Fig. 3B1, B2, B3). The phosphotungstic acid stains positively charged PEI-siRNA polyplex (Fig. 3B1) to a greater extent than the negatively charged liposomes (Fig. 3B2). The lipopolyplex (Fig. 3B3) displays the darker PEI-siRNA complexes in the liposome core. The observed images show the encapsulation of the PEI-siRNA polyplex.

Cellular toxicity studies

Hemolysis assay using rat RBCs

The hemolytic potential of the optimized LPPs and PEI-siRNA polyplexes was analyzed by hemolysis assay. siRNA at quantities 10–100 pmol within the complexes (ratios of liposomes and PEI were equivalent at all siRNA quantities)

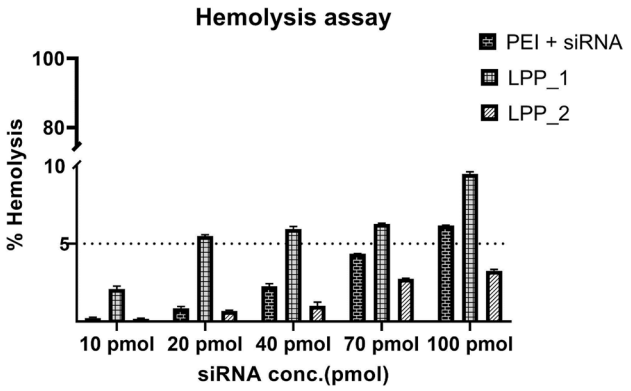

Fig. 4 Hemolysis assay performed at different doses of siRNA. Each bar represents the mean ± SEM (standard error of mean) of three experiments

was incubated with rat RBCs in HBG buffer at 37 °C for 4 h. At 100 pmol siRNA, LPP_1 showed ~ 10% hemolysis of RBCs (as per the release of haem protein measured at 540 nm) relative to the hemolysis of the positive control (triton X-100 equivalent to 100% hemolysis) (Fig. 4). LPP_2 caused less than 4% hemolysis of the rat RBCs at 100 pmol siRNA. This proved that lipidation of PEI-siRNA polyplex by liposome 2 reduced the toxicity of the polyplex.

Cell viability assay: MTT assay

The LPPs and their parent polyplex have been analyzed for their toxicity in ARPE-19 cells. siRNA in increasing quantities (1–10 pmol of siRNA) within the complexes (maintained at equivalent ratios of PEI and liposomes in LPPs) was incubated with ARPE-19 cells for 4 and 24 h at cell culture conditions. It was observed that the LPPs and PEI-siRNA polyplex maintained the cell viability above 70% after 4 h of incubation time at all siRNA quantities, as shown in Fig. 5A, whereas after 24 h of incubation, LPP_1 reduced cell viability to nearly 60% at 10 pmol siRNA (Fig. 5B). Cell viability was retained above 70% at all siRNA quantities formulated as LPP_2. Since LPP_2 maintained better cell viabilities at all siRNA quantities within the complex, as seen by the hemolytic and MTT assays, it was selected over LPP_1 for further analysis in assays for delivery of siRNA to the cell interiors.

In vitro cell uptake study

Flow cytometry

In vitro cellular uptake of PEI polyplex and LPP_2 was studied in ARPE-19 cells using fluorescent-labeled siRNA

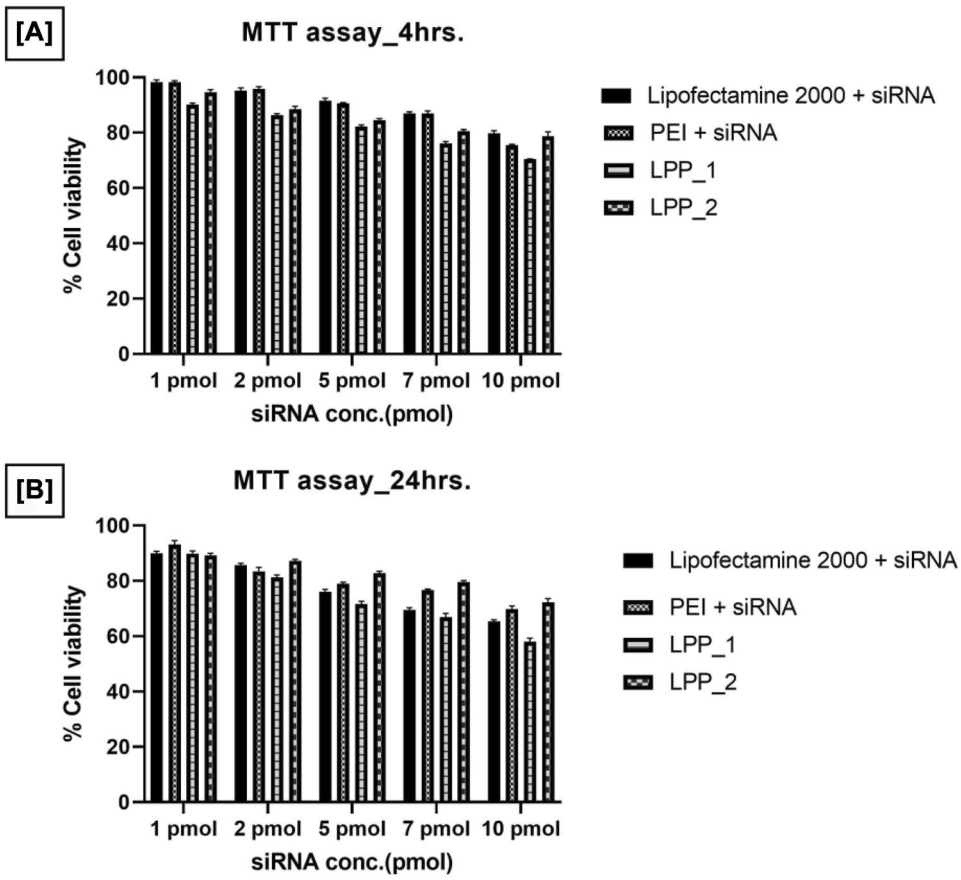

Fig. 5 Cell viability studies with ARPE-19 cells by MTT assay. Cells were incubated for 4 (**A**) and 24 h (**B**) with LPPs (lipopolyplexes) or PEI + siRNA (polyplex), or Lipofectamine 2000 + siRNA, and viability was determined using the MTT test ($n = 5$)

(FAM-siRNA) by flow cytometry. For each sample, 10,000 events were collected. Living cells were selected for analysis by gating the major cell population. Only these cells were analyzed. Comparisons were made with the values obtained by transfections with commercial transfecting agent Lipofectamine 2000 and naked FAM-siRNA. Flow cytometry profiles are shown in Fig. 6A. Compared to untreated cells or those treated with uncomplexed FAM-siRNA, all formulations resulted in a significant increase in mean fluorescence intensity (MFI). The MFI in cells after treatment with various siRNA formulations are illustrated in the histogram depicted (Fig. 6B) as mentioned: Naked siRNA < LPP_2-siRNA < PEI-siRNA polyplex < Lipofectamine2000-siRNA. As shown in Fig. 6B, PEI-siRNA polyplex showed ~79.65% of cell uptake, nearly the same as Lipofectamine 2000, i.e., ~79.35%, whereas LPP_2 showed ~ 75.9% of cell uptake. The percentage of fluorescence-positive cells was calculated as the number of fluorescent events divided by the total number of events in the gate of living cells.

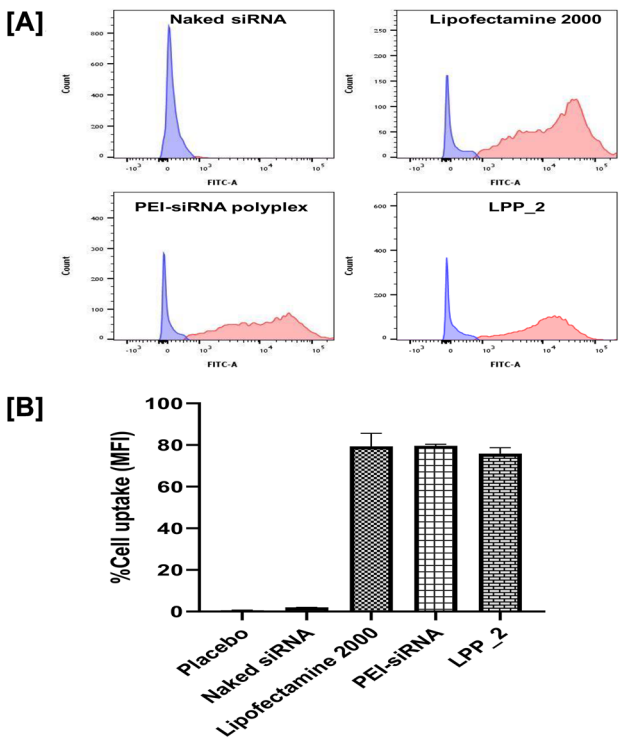

Fig. 6 Flow cytometric studies on cell uptake of FAM-siRNA formulations reflected in MFI (mean fluorescence intensities). **A** Intracellular uptake of naked FAM-siRNA and encapsulated in Lipofectamine 2000, PEI polyplex, and LPP_2 was analyzed using flow cytometry. Please note that all the representative raw images are not at similar scales (*Y*-axis). **B** Histogram on the intracellular uptake of FAM-labeled siRNA in ARPE-19 cells using various delivery vectors. The data reflects the values of three independent experiments

Confocal microscopy

Confocal laser scanning microscopy was used to visualize the subcellular distribution of FAM-siRNA loaded in the ternary complexes. After 4 h of incubation, naked siRNA gave almost no detectable fluorescence in cells (Fig. 7), confirming poor cellular uptake. In comparison, PEI-siRNA polyplex and LPP_2 showed much higher cellular uptake levels of FAM-siRNA. FAM-siRNA was uniformly localized around the nucleus (blue), confirming its cellular entry. Confocal microscopy demonstrated the ability of PEI-siRNA polyplexes and LPPs to enhance intracellular delivery of siRNA.

Gene downregulation studies (in vitro)

Real-time PCR (HuR downregulation)

ARPE-19 cells were transfected with polymer-siRNA and lipid polymer-siRNA complexes containing 50 pmol, 100 pmol, and 150 pmol of scrambled siRNA/HuR siRNA. Table 4 shows the analysis of the transcript levels of HuR. The histogram, Fig. 8A, illustrates the reduction in HuR transcripts on transfection with complexes containing HuR siRNA relative to the untransfected (control) cells. Transfection with scrambled siRNA (Sc) containing complexes did not result in a reduction in HuR transcripts. Thus, the reduction in the HuR transcript levels could be specifically attributed to the designed HuR siRNA used in the study.

Western blotting

To further confirm the results obtained above, western blotting was performed to validate the gene silencing by these selected formulations (Fig. 9A–C). Semi-quantification of the bands by densitometry analysis showed a downregulation of HuR protein expression by PEI -HuR siRNA polyplex and LPP_2 -HuR siRNA at all doses of siRNA used. The transfection with carriers complexed with Sc siRNA did not result in significant downregulation or upregulation of HuR protein.

Quantification of VEGF protein (ELISA technique)

To analyze the effect of HuR protein downregulation on VEGF protein levels, VEGF protein levels were analyzed using ELISA. Dose-dependent reduction in VEGF levels was observed after transfecting the ARPE-19 cells with PEI + HuR siRNA, LPP_2 + HuR siRNA, and Lipofectamine 2000 + HuR siRNA with 50, 100, and 150 pmol of siRNA, as shown in Fig. 8B and Table 5.

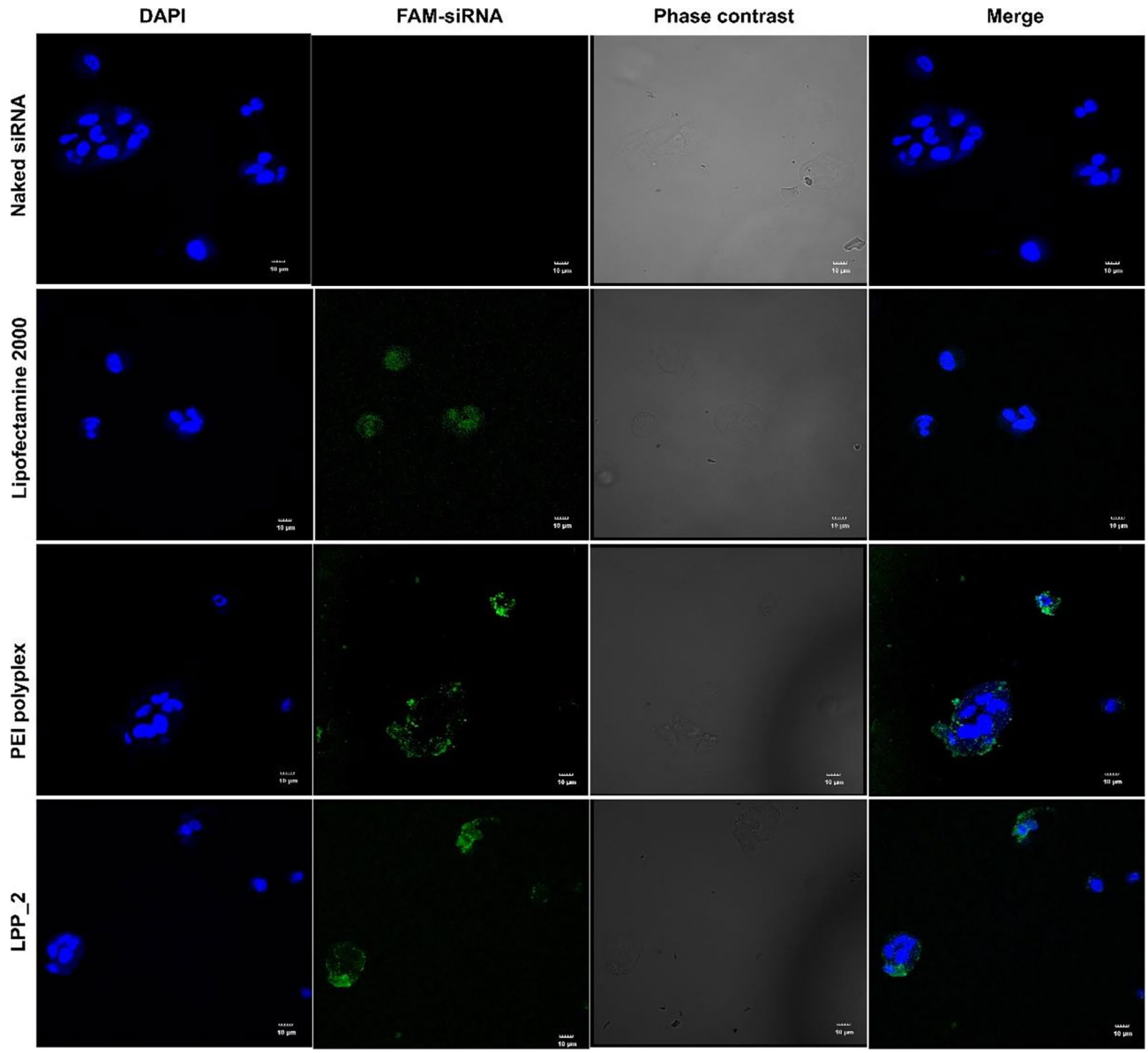

Fig. 7 In vitro cell uptake study in ARPE-19 cells by confocal microscopy. Confocal microscopy was used to study intracellular localization of 100 pmol of FAM-labeled siRNA uncomplexed or complexed with PEI polyplex, LPP_2, and Lipofectamine 2000

Animal studies

The in vivo efficiency study was performed by injecting rat HuR siRNA encapsulated in PEI polyplex, LPP_2, into the STZ-induced diabetic rats intravitreally. A dose of 2.5 pmol/μL (i.e., 2.5 μM) of rat HuR siRNA was selected based on a study conducted by Amadio and co-workers [22]. Triamcinolone is a readily available corticosteroid used for treating DR; hence, it was used for comparison purposes. HuR transcripts and protein (Fig. 10A and B) were upregulated in disease control animals compared to those in which STZ was not administered (i.e., disease-free control). It has been observed that PEI and LPP-2 complexed with rat HuR siRNA could contain the increase in HuR levels seen in the disease control animals, wherein the levels of HuR transcripts increased 2.5-fold relative to the rats in which DR had not been induced, i.e., disease-free animals as shown in Fig. 10B and Table 6. The treatment with HuR siRNA formulations could also significantly restrict the increase in HuR protein levels in untreated disease control (STZ) animals (Fig. 10A). VEGF protein levels, as obtained by the ELISA method, were also contained in the rat HuR siRNA–treated animals compared to the untreated disease control (Fig. 10C). VEGF levels in DC animals were at 472.54 ± 9.83 pg/mg of total protein, and disease-free animals had a normal VEGF

Table 4 Gene expression estimated by real-time PCR by the $2^{-\Delta\Delta Ct}$ method [58]

Formulations + siRNA	Gene expression of HuR with respect to untransfected cells (control cells) at different siRNA doses reflected as $1/2^{-\Delta\Delta Ct}$ values		
	50 pmol	100 pmol	150 pmol
Lipofectamine 2000 + Sc siRNA	1.03 ± 0.03 fold decrease	1.08 ± 0.04 fold decrease	1.05 ± 0.01 fold decrease
Lipofectamine 2000 + HuR siRNA	4.00 ± 0.25 fold decrease	10.27 ± 2.35 fold decrease	13.39 ± 3.54 fold decrease
PEI polyplex + Sc siRNA	1.05 ± 0.05 fold decrease	1.04 ± 0.03 fold decrease	1.07 ± 0.04 fold decrease
PEI polyplex + HuR siRNA	3.50 ± 0.36 fold decrease	7.67 ± 2.96 fold decrease	10.09 ± 1.26 fold decrease
LPP_2 + Sc siRNA	1.05 ± 0.02 fold decrease	1.06 ± 0.06 fold decrease	1.05 ± 0.04 fold decrease
LPP_2 + HuR siRNA	3.20 ± 0.21 fold decrease	4.32 ± 0.49 fold decrease	9.00 ± 1.74 fold decrease

The values are averages of three measurements ± standard deviations (SD)

content in rat retinal tissue of 203.38 ± 8.59 pg/mg of total tissue protein. Treatment with HuR siRNA formulations reduced VEGF levels in retina of rats with DR. PEI-HuR siRNA could reduce VEGF levels to 320.04 ± 9.07 pg/mg of total protein and LPP_2-HuR siRNA restricted VEGF levels to 424.21 ± 29.62 pg/mg of total protein. Comparatively, TRIM treatment reduced VEGF protein levels to 393.38 ± 44.49 pg of VEGF/mg of total tissue protein. Though the VEGF levels attained by treatment were not reduced to normal VEGF levels as seen in the disease-free

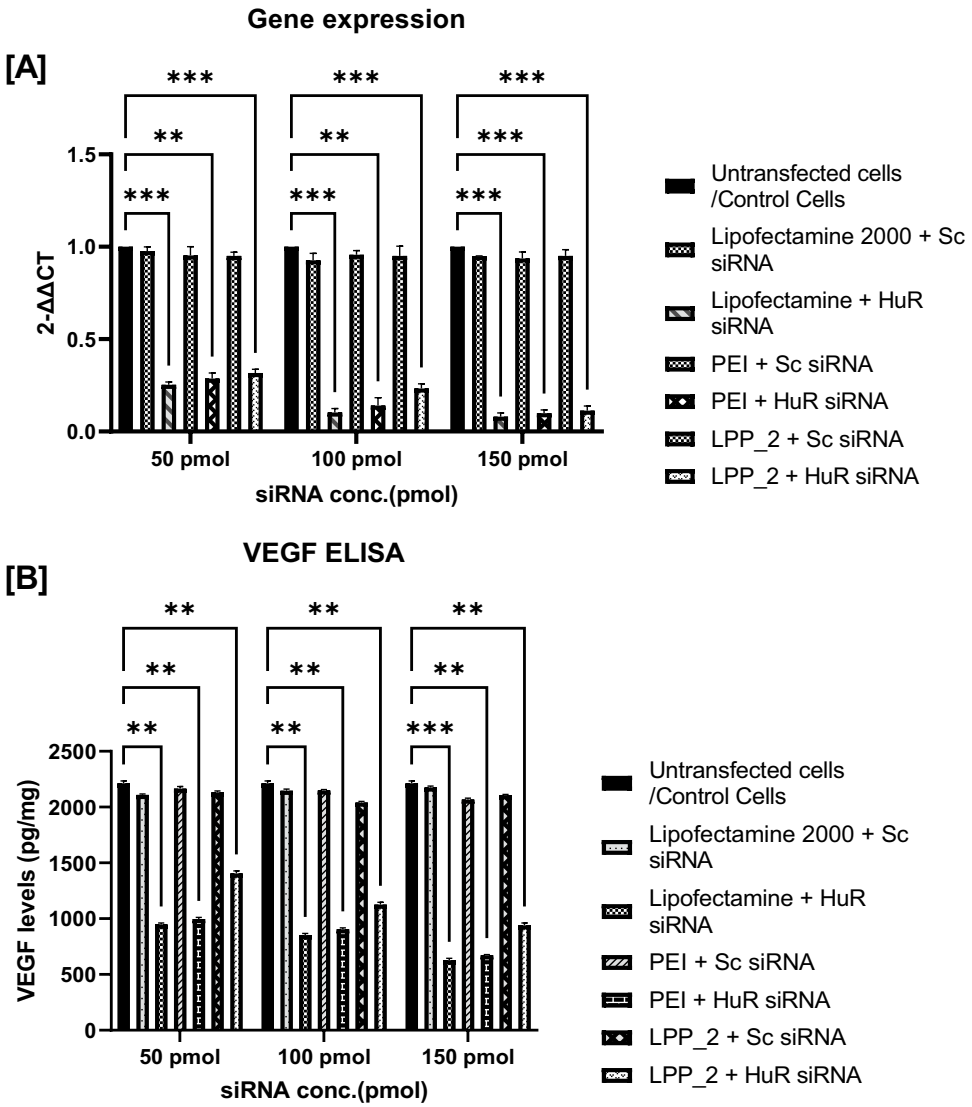

Fig. 8 In vitro downregulation studies employing HuR siRNA. **A** Real-time PCR results. Real-time PCR for analysis of the downregulation of the target gene HuR on transfection with Lipofectamine 2000, polymer, and lipidated polymer (LPP_2) as carriers of HuR siRNA ($n = 3$). The analysis was carried out by the $2.^{-\Delta\Delta Ct}$ method using GAPDH as the housekeeping gene since the PCR efficiency for both genes HuR and GAPDH was found to be comparable. All the formulations were complexed with either HuR targeting siRNA or scrambled siRNA (Sc) and used to transfect ARPE-19 cells, and after 48 h, the reduction in HuR transcript was analyzed. **B** VEGF levels in ARPE-19 cells (pg of VEGF/mg of cellular protein) after 48 h post-transfection were measured via ELISA ($n = 2$) (**$p < 0.001$ vs. untransfected (control) cells, ***$p < 0.0001$ vs. untransfected (control) cells)

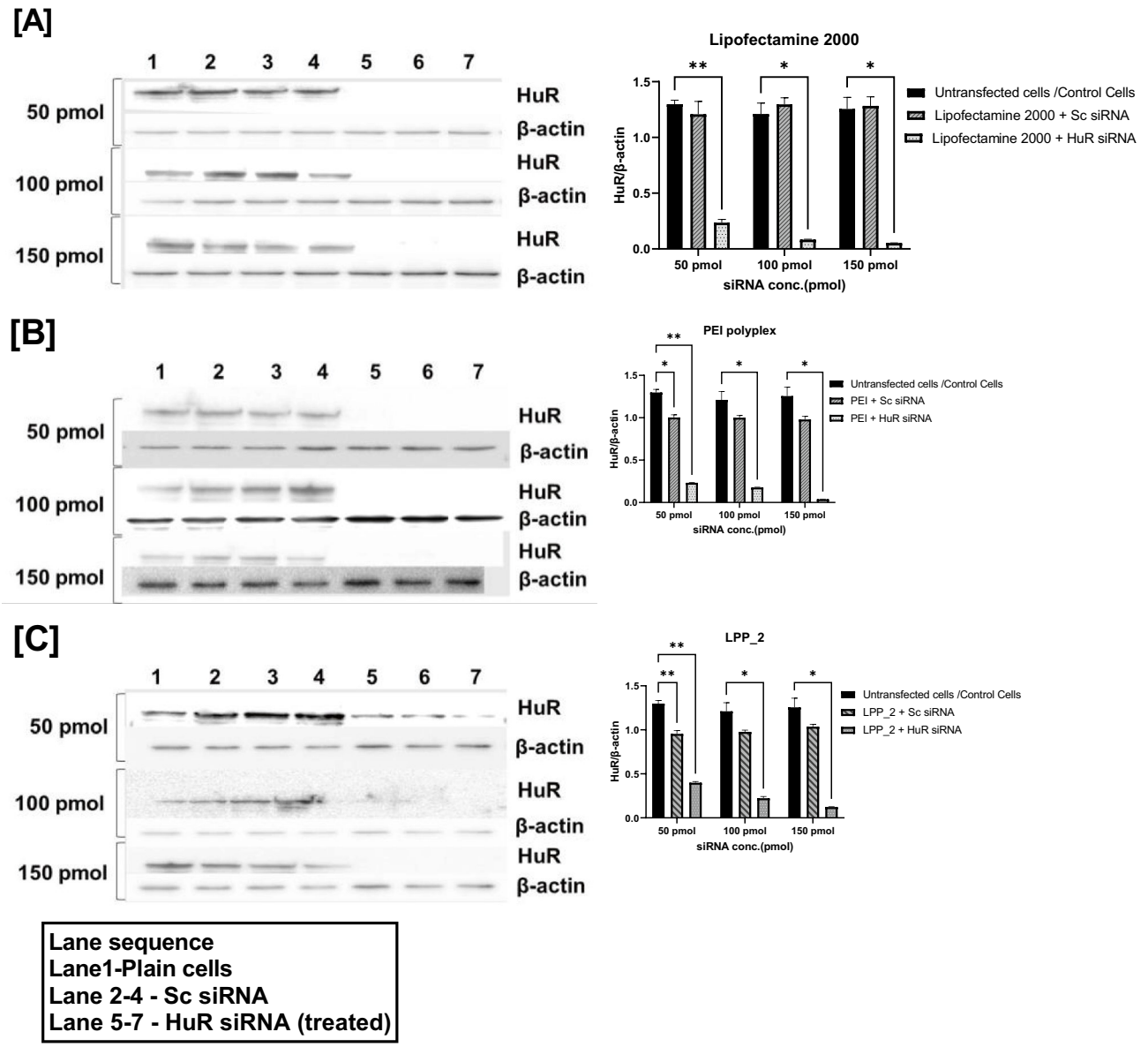

Fig. 9 Western blotting for detecting downregulation of HuR protein expression after transfection of ARPE-19 cells. HuR protein expression on delivery of HuR siRNA mediated by (**A**) Lipofectamine 2000, (**B**) PEI, and (**C**), LPP_2, and at three siRNA doses, i.e., 50, 100, and 150 pmol, are shown. The transfections were carried out in triplicate. The representative western blot images are presented, and on the right side, the densitometry analysis of the western blot (mean ± SEM) of HuR/β-actin is mentioned for the respective blot. The mean gray levels measured by Image J software; $*p<0.01$, $**p<0.001$, $***p<0.0001$ vs. plain cells. Each blot contains the triplicate bands from three different transfections, and the average comparative band intensity of these three bands is mentioned in the mean gray levels (on the left side of the blot). Lane sequences, Lane 1—plane cells, Lanes 2 to 4—scrambled siRNA complexed with Lipofectamine 2000 or PEI or LPP_2, Lanes 5 to 7—Lipofectamine 2000 or PEI or LPP_2 complexed with HuR siRNA

rats, the VEGF levels were significantly lower as compared to the untreated disease control animals.

Fundoscopic images

During clinical evaluation, no ocular damage such as corneal edema, hyperemia or conjunctival secretion, hemorrhaging, vitreous opacity, or retinal detachment was observed after the intravitreal injection. Ocular fundus examinations were performed on each animal group and registered as representative images, as shown in Fig. 11. Fundoscopic examination revealed that the untreated control rat eye showed a clear retinal center, macula, and retinal vessels, whereas the STZ rat eye displayed inflammation, redness at the center of the retina, and retinal vascular tortuosity. Images after siRNA treatment and marketed formulation administration show reduced inflammation and neovascularization to some extent, compared to STZ-treated rat eye, as seen in Fig. 11.

Table 5 VEGF protein levels in ARPE 19 cells determined by VEGF ELISA

Formulations + siRNA	VEGF pg/mg of cellular protein on the transfection of ARPE-19 cells with carriers of HuR siRNA/scrambled siRNA (Sc siRNA) at different doses		
	50 pmol siRNA	100 pmol siRNA	150 pmol siRNA
Untransfected cells/control cells	2214.33 ± 28.28 pg/mg		
Lipofectamine 2000 + Sc siRNA	2064.33 ± 28.30 pg/mg	2147.67 ± 18.86 pg/mg	2176.00 ± 16.50 pg/mg
Lipofectamine 2000 + HuR siRNA	949.33 ± 16.50 pg/mg	852.67 ± 21.21 pg/mg	627.67 ± 23.57 pg/mg
PEI polyplex + Sc siRNA	2166.00 ± 25.93 pg/mg	2091.00 ± 18.90 pg/mg	2149.33 ± 11.79 pg/mg
PEI polyplex + HuR siRNA	996 ± 21.21 pg/mg	906 ± 16.50 pg/mg	671 ± 9.43 pg/mg
LPP_2 + Sc siRNA	2132.67 ± 16.50 pg/mg	2041.00 ± 14.14 pg/mg	2107.67 ± 9.43 pg/mg
LPP_2 + HuR siRNA	1406.00 ± 30.64 pg/mg	1126 ± 30.64 pg/mg	941 ± 28.28 pg/mg

The values are averages of three measurements ± standard deviations (SD)

Histological studies

The rat retinal tissue shows four well-structured retinal layers ganglion cell layer (GCL), inner plexiform layer (IPL), inner nuclear layer (INL), and outer retinal layer (ORL). Densely packed cells in GCL and ORL are observed in control/disease-free rat retina (Fig. 12A), whereas DC or untreated rat retina, in comparison, showed distorted ORL (Fig. 12B). The treatment with HuR rat siRNA and TRIM reduces the continued distortion of ORL due to DR to some extent, as shown in Fig. 12C, D, and E.

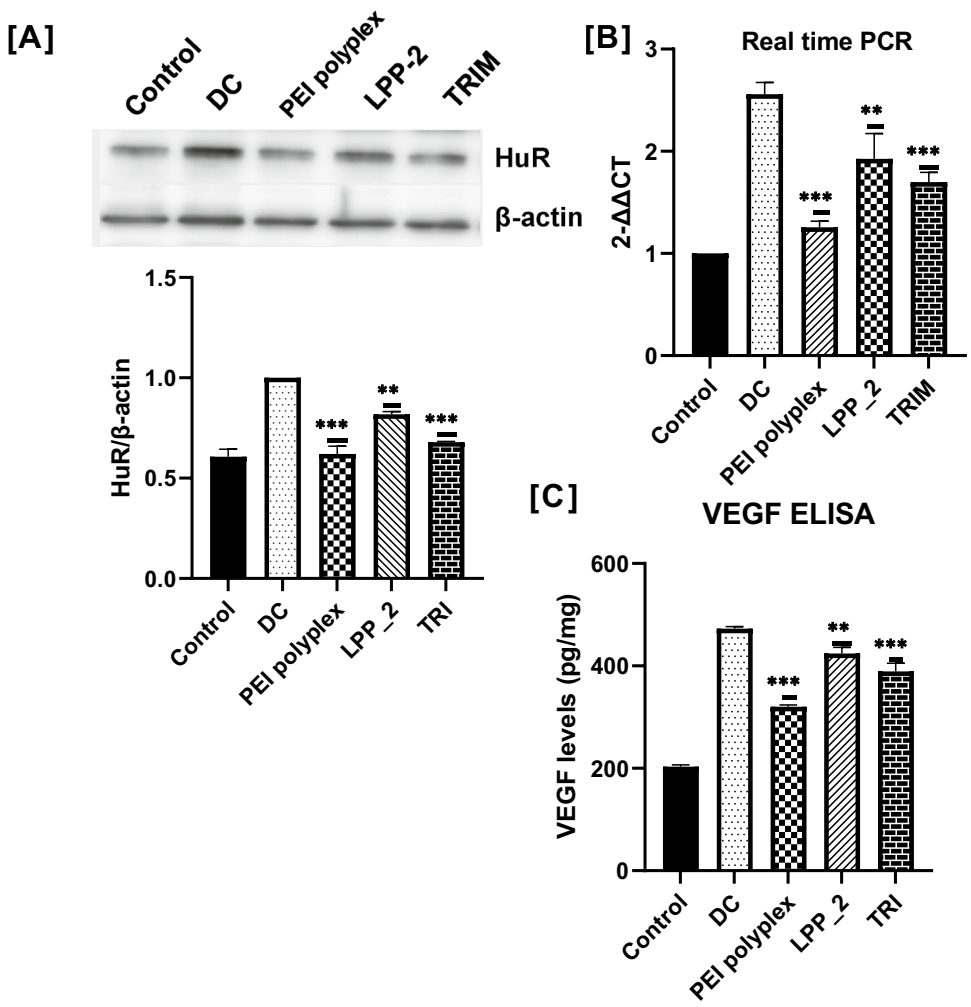

Fig. 10 In vivo efficacy study of the siRNA formulations in the STZ-induced rat model. **A** Representative image of the western blotting and densitometry analysis of the western blot (mean ± SEM). The mean gray levels were measured by Image J software. **B** The gene expression levels of the HuR mRNA after treatment with HuR siRNA containing PEI polyplex, LPP_2, and the drug triamcinolone acetate. **C** VEGF levels in the rat retinal tissue expressed as pg/mg of total protein. *$p < 0.01$, **$p < 0.001$, ***$p < 0.0001$ vs. DC (disease control, i.e., untreated STZ rats) ($n = 6$)

Table 6 Gene expression estimated by real-time PCR by the $2^{-\Delta\Delta Ct}$ method in rat retinal tissue

Formulations + HuR rat siRNA	Gene expression of HuR with respect to control/disease-free animals ($2^{-\Delta\Delta Ct}$)
Disease control (DC/STZ only)	2.56 ± 0.28 fold increase
PEI polyplex + rat HuR siRNA	1.26 ± 0.15 fold increase
LPP_2 + rat HuR siRNA	1.93 ± 0.61 fold increase
TRIM	1.7 ± 0.23 fold increase

Discussion

The eye is anatomically divided into two broad segments: the anterior segment comprises the iris, ciliary body, cornea, lens, and surrounding aqueous humor, while the posterior segment includes the sclera, choroid, retina, Bruch's membrane, vitreous humor, and the optic nerve [59]. Ocular diseases of the posterior segment of the eye contribute to visual impairment, which may result in blindness in nearly 100 million affected people [60]. The posterior section of the eye is difficult to access; hence, for treatment, medications may be delivered by topical, intravitreal, periocular, or systemic routes, depending on the disease type, drug, and target site. The posterior portion of the eye has distinct morphological, physiological, and biochemical barriers that protect the eye against a variety of harmful exposures [61, 62]. Over the last decade, intravitreal injection has become a standard and effective treatment for posterior segment diseases, breaking down obstacles to drug delivery [63]. Through the intraocular route, the drug is placed directly in the vitreous humor. The route is invasive but popular due to the reduction of systemic exposure to the medication [63]. Therapeutics can be administered into the vitreous through simple injection with a high-gauge needle, resulting in therapeutic intraocular drug concentrations locally surrounding the retinal tissues while limiting off-target exposure [64] and systemic side effects. However, most intravitreally administered drugs are of short to medium duration due to the existence of dynamic clearance mechanisms in the eye [65]. As a result, the frequency of administration is high to maintain adequate intraocular drug concentrations, posing a burden to the caregiver and patient. In addition, the large number of intravitreal injections for chronic disease can lead to adverse events, including endophthalmitis, hemorrhage, retinal detachment, and glaucoma[66]. Despite the disadvantages, this route is preferred since it provides direct, local treatment [67]. To reduce the frequency of injections, the drug formulations need to be modified with respect to size, charge, and lipophilicity [68].

Nucleic acid drugs are being increasingly investigated to treat posterior segment eye diseases. Among these siRNAs, therapeutics are popular candidates. Bevasiranib, a siRNA-based anti-angiogenic agent, is undergoing clinical trials (phase 3) to treat wet age-related macular degeneration in combination with ranibizumab (NCT00499590). Nanoparticular formulations are advantageous for the delivery of nucleic acids that require intracellular delivery into retinal

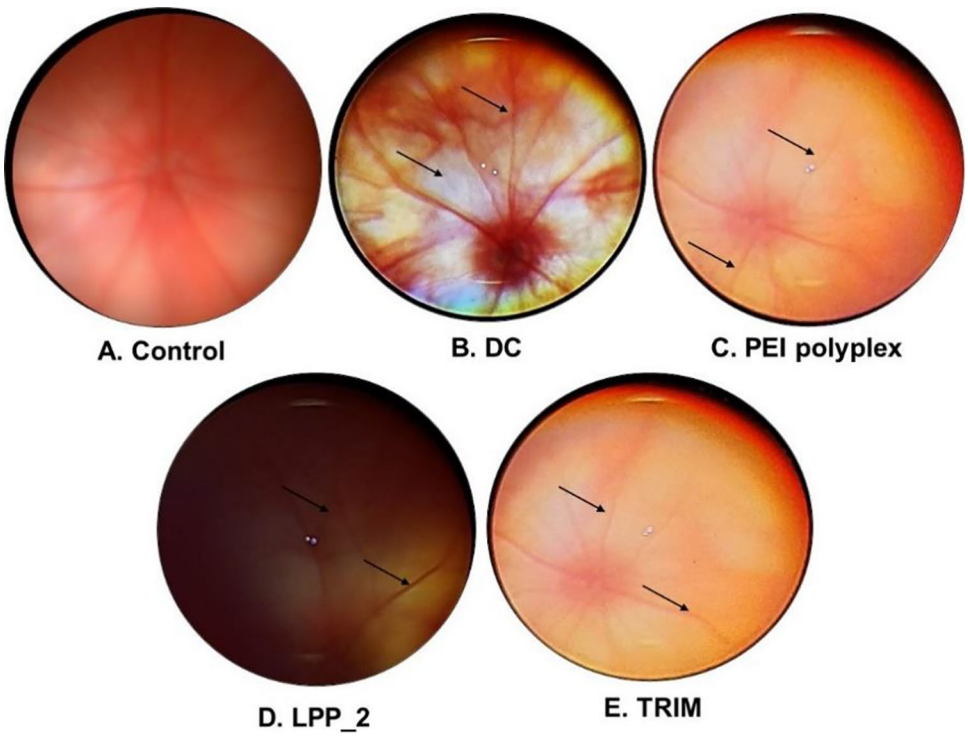

Fig. 11 Representative images of ocular fundus examinations after intravitreal injection of saline in control and DC (STZ control), and intravitreal administration of PEI polyplex (containing HuR siRNA), LPP_2 (containing HuR siRNA), and TRIM (triamcinolone acetate)

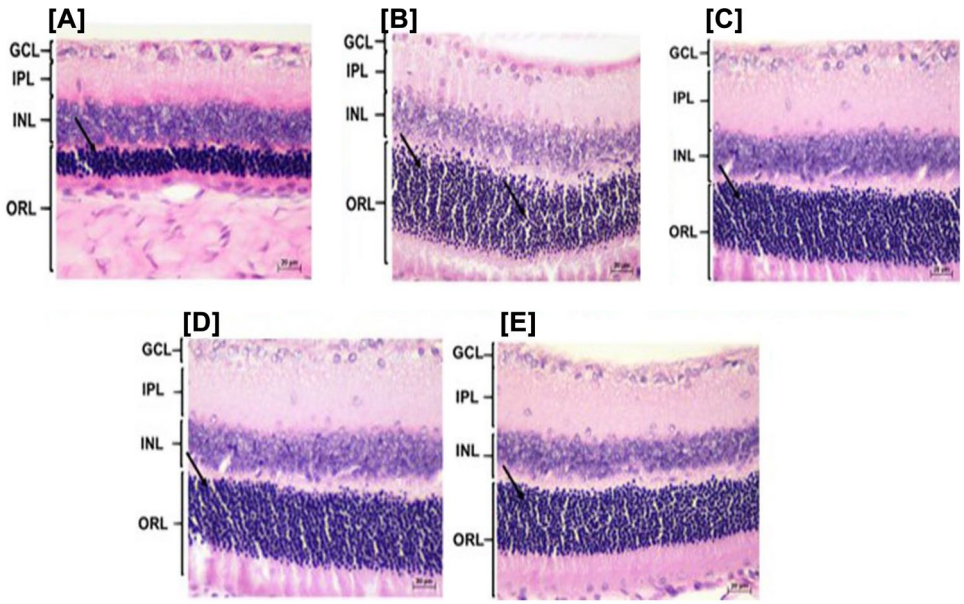

Fig. 12 Effect of intravitreal siRNA treatment on rat retinal histopathology. Representative histopathology micrographs of (**A**) control rat retina, (**B**) DC (STZ treated only), (**C**) PEI polyplex (STZ + PEI-HuR siRNA polyplex), (**D**) LPP_2 (STZ + LPP_2-HuR siRNA), and (**E**) TRIM (STZ + TRIM). The images show hematoxylin–eosin-stained (H-E stained) paraffin-embedded retina sections. Retinal layers are indicated on the left part of the figure: GCL, ganglion cell layer; IPL, inner plexiform layer; INL, inner nuclear layer, and ORL, outer retinal layer (comprises of outer plexiform layer; outer nuclear layer; and photoreceptor layer). The ORL layer (indicated by a black arrow) is distorted in the streptozotocin treated rats (Images **B**, **C**, **D**, **E**) as compared to the control untreated rats (Image A). The distortion of ORL observed in images (**C**, **D**, **E**) is suppressed to some extent on administration of HuR siRNA/TRIM

cells. Nanoparticles may increase the bioavailability of the drug in ocular tissue, its retention time, efficacy, patient comfort, and compliance [69]. The ocular barriers to the successful delivery of formulations to the retinal tissues through the intravitreal route are vitreous humor and vitreoretinal interface (composed of cortical vitreous, inner limiting membrane (ILM), Muller cell footplates) [70–72].

The vitreous contains water (98%), colloids (0.1%), ions, and low molecular weight solutes. It is a complex three-dimensional structure of collagens, glycosaminoglycans (GAGs), and non-collagenous structural proteins[73]. GAGs, hyaluronan, and heparan sulfate (components of vitreous) interact with nucleic acids enclosed in polymers and liposomes [74]. The vitreous restricts the movement of nanoparticles by acting as a charged (anionic) molecular sieve [74]. Vitreal mobility and retention times of nanoparticles are a function of nanoparticular size and charge [69, 74–76]. Anionic and neutral formulations were found to be mobile whereas cationic particles were immobilized in the vitreous [69]. Large neutral nanoparticles (> 200 nm) had reduced diffusion [69]. PEGylation was found to increase the mobility of cationic and large neutral formulations with little effect on anionic and smaller neutral particles [69].

Synthetic polymers such as PEI, PLL (poly-L lysine), and PLGA (poly(lactide-co-glycolide) have been investigated for ocular gene delivery [77]. However, when solely used for delivery, they are associated with cellular toxicity, short intravitreal half-life, and transient gene expression [77]. Liposomes are formed by the self-assembly of lipid molecules, each having a hydrophilic head group and a hydrophobic tail. As active moiety carriers, they exhibit favorable properties such as protection of the encapsulated drug, controlled drug release, biocompatibility, improvised active/passive targeting, and improving therapeutic benefits [78]. Lipid polymer hybrids unite unique characteristics of liposomes and polymers, making them exciting drug carriers [79].

The combination of liposomes and cationic polymers has been particularly appealing earlier because it encompasses the advantageous features of both constituents for nucleic acid delivery [80, 81]. Among the various cationic polymers, PEI is widely used for the delivery of nucleic acids, especially after being reported for the first time in 1995 by Boussif et al. [82]. These can be synthetically prepared as branched (bPEI) or linear (lPEI) polymers with a wide variety of molecular weights. lPEI has secondary amines in the backbone and primary amines at the polymer ends, whereas bPEI has a 1:2:1 ratio of primary, secondary, and tertiary amine groups, which strongly increases the polymer's buffering capacity [83]. However, bPEI reduces cell viability on transfection; therefore, low MW (5–48 kDa) is preferred [77].

In our study, bPEI of average MW 25 K was employed as the polymer of choice for siRNA complexation. The bPEI: siRNA polyplex at an N/P ratio of 20:1 yielded a size of 207 nm and an average zeta potential of ~ 10 mV (Table 3). Subsequently, the polyplex was mixed with hydrated lipid vesicles (liposomes) composed of DPPC, HSPC, cholesterol, and mPEG 2000-DSPE with/without DOPE to give lipopolyplexes (LPP_1 (without DOPE), LPP_2 (with DOPE)). The lipid vesicles were composed of neutral lipids DPPC (Tm = 41 °C), HSPC (Tm = 52 °C), Cholesterol, DOPE (Tm = −16 °C), and DSPE [84]. The liposomes formed were mildly anionic in nature as reflected by their negative zeta potentials (average values, −8.35 mV and −7.31 mV). The charge on the liposomes may be due to the negative charge of mPEG 2000-DSPE in aqueous solutions at neutral pH, due to ionization of the phosphate groups [85]. The LPPs formed after the inclusion of the polyplex were weakly cationic (Table 3), with the differences between the zeta potential of the polyplex and the lipopolyplex being insignificant. The sizes of the polyplex and the lipopolyplexes were within 200–260 nm, which was suitable for ocular delivery. The nearly neutral, large (> 200 nm) LPPs contained PEG 2000 to aid diffusion across the vitreous in vivo, to reduce aggregation, and to increase stability. Initially, the formulations were evaluated in vitro for their ability to protect their payload against serum components, RNases, and heparin (a polyanion structurally similar to heparan sulfate [86]. Heparin, as a polyanion, competes with cationic complexes and displaces condensed DNA/siRNA [87]. Both the LPPs protected the nucleic acids against serum components and RNAse A and were stable in the presence of heparin doses up to 2 IU (Fig. 1). The polyplex was however unstable in the presence of 0.25 IU heparin and released the siRNA. Thus, lipidation of the polyplex could stabilize the formulation in the presence of other anions (Fig. 2B). Lipidation of the polyplex also caused an increase in the efficiency of siRNA encapsulation (Fig. 2A). Among the LPPs, LPP_2 showed better properties with respect to LPP_1 in heparin assays and in vitro cytotoxicity tests (Figs. 4 and 5). The hemolysis assay, which exposed rat RBCs to polyplexes and LPPs with increasing equimolar doses of siRNA, revealed that LPP_1 had high hemolytic potential (Fig. 4). Cell viability assays performed on ARPE-19 cells showed reduced viability with LPP_1 compared to the naked polyplex and LPP_2. LPP_1 has phospholipids with high transition temperatures (Tm) compared to LPP_2, in which DOPE has been incorporated. The toxicity of LPP_1 over LPP_2 may be attributed to its greater rigidity. Because of its inherent toxicity, LPP_1 was not evaluated in further experiments.

The hypothesis that HuR siRNA downregulates HuR protein with concomitant reduction of the VEGF protein was proved by Amadio and colleagues in the rat retinal system [19, 22]. We observed a similar trend in human retinal pigment epithelial cells (ARPE-19) when transfected with the designed siRNA against human HuR mRNA. The rat HuR mRNA (NM_001108848.1) contains 2439 ribonucleotides, while the human HuR mRNA (NM_001419.3) is composed of 6054 ribonucleotides. Transfection of ARPE-19 cells with the polyplex and LPP_2 (containing human HuR siRNA) resulted in the downregulation of HuR mRNA, HuR protein, and VEGF protein (Tables 4, 5, Fig. 9). Thus, we could prove this hypothesis in the human retinal system with our designed siRNA specific for human HuR mRNA.

The observations made after 48 h of transfection of ARPE-19 cells showed that polyplexes were more efficient in downregulating HuR mRNA and VEGF protein than lipopolyplexes. This finding cannot be attributed to differences in uptake since flow cytometric results showed similar transfection potential of the polyplexes and lipopolyplexes (Fig. 6). PEG in cationic liposomes has been found to inhibit the release of its nucleic acid payload from endosomes previously [88]. Song and colleagues also proposed that the delay in the release of plasmid DNA components from the PEG-liposomes may increase DNA vulnerability to degradation since their liposomes could only partially protect the nucleic acid from DNases [88]. But we hypothesize that the grafting of mPEG 2000-DSPE in our liposomes may contribute to the sustained release of siRNA from the lipopolyplex compared to the naked polyplex.

DR arises due to high and fluctuating glycemic levels in patients with DM. Control of blood glucose in DM patients may aid preventing or ameliorating DR progression [30]. The implication of VEGF-A in the pathogenesis of DR led to the emergence of therapeutics targeting this factor. Before the advent of intravitreally administered anti-VEGF agents, treatment of DR consisted of laser photocoagulation and control of systemic factors [89].

Animal studies were carried out on an STZ-induced diabetic rat as a model of DR. STZ dose to induce type 1 DM was 55 mg/kg as a single intraperitoneal dose. At higher doses (100 mg/kg), STZ can cause the animal to develop severe diabetes with concomitant lethal diabetic ketoacidosis, and smaller doses (≤ 25 mg/kg) can cause the animal to develop mild transient glycosuria [90]. In Wistar rats, induction of DM occurs 3 days post STZ injection, as observed in our study [91]. The animals were given sufficient food and water to avoid their untimely demise by diabetic ketoacidosis. Fundoscopic examinations confirmed the onset of DR, 25 days post-induction, and treatment with HuR siRNA was initiated. TRIM, used in the treatment of advanced DR [92, 93], was employed for comparisons with the HuR siRNA treatment as a positive drug control in one of the treatment groups. The HuR siRNA used for this study was identical to that employed by Amadio and colleagues [22] since the efficacy of the sequence to downregulate HuR had been proved. Real-time PCR results revealed the upregulation of

the HuR mRNA in the STZ disease control group, proving that HuR is indeed overexpressed in DR (Fig. 10, Table 6), similar to the observation by Amadio and colleagues [22]. The treatment with HuR siRNA or TRIM could not bring back the levels of the RBP to that seen in the disease-free control group, though the levels were intermediate to the disease-free and disease control groups as observed in the TRIM and LPP_2-HuR siRNA-treated groups, except for the PEI-HuR siRNA group where HuR expression was halved compared to the disease control (Table 6).

The ELISA study also revealed a significant decrease in VEGF protein in the PEI-HuR siRNA group (320 pg/mg of retinal tissue) compared to the disease control group (472 pg/mg) and the LPP_2-HuR siRNA group (424 pg/mg of retinal tissue) (Fig. 10). The studies revealed that PEI could achieve better downregulation of the target genes in vivo compared to the lipopolyplexes used in the study. These findings conform to those obtained in vitro using ARPE-19 cells where the PEI-siRNA carrier could achieve better downregulation of HuR and VEGF. This finding is contrary to that obtained by Reddy and colleagues[81] when they compared similar siRNA formulations in luciferase-expressing human adenocarcinoma cells for downregulating luciferase. The inclusion of mPEG 2000-DSPE in our lipopolyplex formulations may be responsible for this difference in results obtained. The transfection efficiency of PEI-siRNA, and LPP_2-siRNA are similar (~75–80%) as observed in flow cytometry experiments on ARPE-19 cells using 6′FAM-siRNA (Fig. 6). The confocal experiments too did not detect any significant differences in the localization of fluorescent siRNA from both the formulations (Fig. 7). However, PEG may contribute to a slow but sustained release of HuR siRNA from the lipopolyplex aqueous core, compared to unlipidated PEI-HuR siRNA, within cells. The inherent proton sponge effect in the naked PEI-HuR siRNA complex may have led to the complete release of the therapeutic payload causing greater downregulation of the targeted moiety as compared to the lipidated (PEG containing) PEI-HuR siRNA. The sustained release of nucleic acid from the lipopolyplex may be advantageous for the reduction of the frequency of intravitreal dosing required for siRNA-based treatment of DR. Our study was terminated 48 h, post intravitreal injection since the primary objective was to study the efficacy of the siRNA-based formulations to reduce the vascularization observed in the retina due to DR. Further studies for longer periods may be initiated in STZ rats with concomitant insulin injections to reduce the distress of the animal. Fundus imaging confirmed the reduction in inflammation and tortuosity of retinal vessels more effectively with treated formulation than disease control (STZ only), as shown in Fig. 11. The intraocular administration of PEI polyplex and LPP_2 containing rat HuR siRNA restrained the changes in retinal layer arrangement, especially GCL, and ORL, as shown in Fig. 12C, D, and E. The formulations containing HuR siRNA were successful in delivering siRNA to the ocular tissues and could ameliorate the destruction of the retina in DR.

Conclusion

In conclusion, lipidation of the PEI polyplex helps in the cytoplasmic delivery of siRNA to cells. TEM experiments reveal the multicomponent polyplex-in-liposome structure of the LPPs. The LPP formulation showed reduced release of the siRNA in vitro and in vivo compared to the polyplex, which may be attributed to a sustained release of the nucleic acid payload from the LPP. Concomitant downregulation of VEGF protein when HuR mRNA is targeted by RNA interference is also observed in the human system. Amelioration of DR in STZ-treated rats on treatment with HuR siRNA LPP formulations suggests its applicability for treatment in human ocular tissues.

Acknowledgements The authors are grateful to the Director of NRRCH, Dr. Geetanjali Sachdeva, for her valuable support and cooperation. The authors appreciate the assistance provided by Mr. Jayant Tare and Mr. Pravin Salunkhe during animal experimentation/histological work at NIRRCH. We are thankful to Dr. S. S Bhatti, Grant Govt. Medical College and Group of Hospitals, Mumbai, India, for rat ophthalmoscopy. The authors are grateful to Dr. Chadrashekhar Mote for technical input and eye histology analysis guidance.

Author contribution Shibani Supe: investigation, methodology, validation, writing—original draft. Archana Upadhya: investigation, methodology, supervision, writing—review and editing. Santosh Tripathi: in vivo experimentation, methodology, validation. Vikas Dighe: resources, supervision, validation, writing. Kavita Singh: conceptualization, supervision, resources, funding acquisition, writing—review and editing.

Funding This research work is outcome of fund received as Early Career Award to Dr. Kavita Singh from Science and Engineering Research Board (SERB/F/9850/2017–2018), Department of Science and Technology, Government of India.

Availability of data and materials The datasets generated during and/or analyzed during the current study are available from the corresponding author on reasonable request.

Declarations

Ethics approval The animal experiments were conducted as per the guidelines of the Committee for the Purpose of Control and Supervision of Experiments on Animals (CPCSEA), India. The study protocol was approved by the Institutional Animal Ethics Committee (IAEC) of NIRRH [Application numbers: NIRRH/IAEC/ 20/20].

Consent to participate Not applicable. Human subjects were not used in this study.

Consent for publication Not applicable.

Conflict of interest The authors declare no competing interests.

References

1. Teo ZL, Tham YC, Yu M, Chee ML, Rim TH, Cheung N, et al. Global prevalence of diabetic retinopathy and projection of burden through 2045: systematic review and meta-analysis. Ophthalmology. 2021;128(11):1580–91. https://doi.org/10.1016/j.ophtha.2021.04.027.
2. Stitt AW, Lois N, Medina RJ, Adamson P, Curtis TM. Advances in our understanding of diabetic retinopathy. Clin Sci (Lond). 2013;125(1):1–17. https://doi.org/10.1042/cs20120588.
3. Wong TY, Cheung CM, Larsen M, Sharma S, Simo R. Diabetic retinopathy Nat Rev Dis Primers. 2016;2:16012. https://doi.org/10.1038/nrdp.2016.12.
4. Zhao Y, Singh RP. The role of anti-vascular endothelial growth factor (anti-VEGF) in the management of proliferative diabetic retinopathy. Drugs Context. 2018;7: 212532. https://doi.org/10.7573/dic.212532.
5. Mathew C, Yunirakasiwi A, Sanjay S. Updates in the management of diabetic macular edema. J Diabetes Res. 2015;2015: 794036. https://doi.org/10.1155/2015/794036.
6. Miller K, Fortun JA. Diabetic macular edema: current understanding, pharmacologic treatment options, and developing therapies. Asia Pac J Ophthalmol (Phila). 2018;7(1):28–35. https://doi.org/10.22608/apo.2017529.
7. Gupta N, Mansoor S, Sharma A, Sapkal A, Sheth J, Falatoonzadeh P, et al. Diabetic retinopathy and VEGF. Open Ophthalmol J. 2013;7:4–10. https://doi.org/10.2174/1874364101307010004.
8. Holecamp NM. Overview of diabetic macular edema. Am J Manag Care. 2016;22:S284–91 (PMID: 27668630).
9. Campochiaro PA, Aiello LP, Rosenfeld PJ. Anti-vascular endothelial growth factor agents in the treatment of retinal disease: from bench to bedside. Ophthalmology. 2016;123(10S):S78–88. https://doi.org/10.1016/j.ophtha.2016.04.056.
10. Pramanik S, Mondal LK, Paine SK, Jain S, Chowdhury S, Ganguly U, et al. Efficacy and cost-effectiveness of anti-VEGF for treating diabetic retinopathy in the Indian population. Clin Ophthalmol. 2021;15:3341–50. https://doi.org/10.2147/opth.s317771.
11. Andreoli CM, Miller JW. Anti-vascular endothelial growth factor therapy for ocular neovascular disease. Curr Opin Ophthalmol. 2007;18(6):502–8. https://doi.org/10.1097/icu.0b013e3282f0ca54.
12. Ferrara N, Adamis AP. Ten years of anti-vascular endothelial growth factor therapy. Nat Rev Drug Discovery. 2016;15(6):385–403. https://doi.org/10.1038/nrd.2015.17.
13. Roy H, Bhardwaj S, Yla-Herttuala S. Biology of vascular endothelial growth factors. FEBS Lett. 2006;580(12):2879–87. https://doi.org/10.1016/j.febslet.2006.03.087.
14. Levy AP, Levy NS, Goldberg MA. Post-transcriptional regulation of vascular endothelial growth factor by hypoxia. J Biol Chem. 1996;271(5):2746–53. https://doi.org/10.1074/jbc.271.5.2746.
15. Levy NS, Chung S, Furneaux H, Levy AP. Hypoxic stabilization of vascular endothelial growth factor mRNA by the RNA-binding protein HuR. J Biol Chem. 1998;273(11):6417–23. https://doi.org/10.1074/jbc.273.11.6417.
16. Osera C, Martindale JL, Amadio M, Kim J, Yang X, Moad CA, et al. Induction of VEGFA mRNA translation by CoCl2 mediated by HuR. RNA Biol. 2015;12(10):1121–30. https://doi.org/10.1080/15476286.2015.1085276.
17. Shang J, Zhao Z. Emerging role of HuR in inflammatory response in kidney diseases. Acta Biochim Biophys Sin (Shanghai). 2017;49(9):753–63. https://doi.org/10.1093/abbs/gmx071.
18. Wang J, Guo Y, Chu H, Guan Y, Bi J, Wang B. Multiple functions of the RNA-binding protein HuR in cancer progression, treatment responses and prognosis. Int J Mol Sci. 2013;14(5):10015–41. https://doi.org/10.3390/ijms140510015.
19. Amadio M, Bucolo C, Leggio GM, Drago F, Govoni S, Pascale A. The PKCbeta/HuR/VEGF pathway in diabetic retinopathy. Biochem Pharmacol. 2010;80(8):1230–7. https://doi.org/10.1016/j.bcp.2010.06.033.
20. Govindaraju S, Lee BS. Adaptive and maladaptive expression of the mRNA regulatory protein HuR. World J Biol Chem. 2013;4(4):111–8. https://doi.org/10.4331/wjbc.v4.i4.111.
21. Goldberg-Cohen I, Furneauxb H, Levy AP. A 40-bp RNA element that mediates stabilization of vascular endothelial growth factor mRNA by HuR. J Biol Chem. 2002;277(16):13635–40. https://doi.org/10.1074/jbc.m108703200.
22. Amadio M, Pascale A, Cupri S, Pignatello R, Osera C, V DA, et al. Nanosystems based on siRNA silencing HuR expression counteract diabetic retinopathy in rat. Pharmacol Res. 2016;111:713–20. https://doi.org/10.1016/j.phrs.2016.07.042.
23. Elbashir SM, Lendeckel W, Tuschl T. RNA interference is mediated by 21- and 22-nucleotide RNAs. Genes Dev. 2001;15(2):188–200. https://doi.org/10.1101/gad.862301.
24. Petit L, Khanna H, Punzo C. Advances in Gene Therapy for Diseases of the Eye. Hum Gene Ther. 2016;27(8):563–79. https://doi.org/10.1089/hum.2016.040.
25. Saraiva SM, Castro-Lopez V, Paneda C, Alonso MJ. Synthetic nanocarriers for the delivery of polynucleotides to the eye. Eur J Pharm Sci. 2017;103:5–18. https://doi.org/10.1016/j.ejps.2017.03.001.
26. Supe S, Upadhya A, Singh K. Role of small interfering RNA (siRNA) in targeting ocular neovascularization: a review. Exp Eye Res. 2021;202. https://doi.org/10.1016/j.exer.2020.108329.
27. Leclercq B, Mejlachowicz D, Behar-Cohen F. Ocular barriers and their influence on gene therapy products delivery. Pharmaceutics. 2022;14(5). https://doi.org/10.3390/pharmaceutics14050998.
28. Sahu B, Chug I, Khanna H. The ocular gene delivery landscape. Biomolecules. 2021;11(8). https://doi.org/10.3390/biom11081135.
29. Bordet T, Behar-Cohen F. Ocular gene therapies in clinical practice: viral vectors and nonviral alternatives. Drug Discov Today. 2019;24(8):1685–93. https://doi.org/10.1016/j.drudis.2019.05.038.
30. Wang JH, Roberts GE, Liu GS. Updates on gene therapy for diabetic retinopathy. Curr Diab Rep. 2020;20(7):22. https://doi.org/10.1007/s11892-020-01308-w.
31. Yin H, Kanasty RL, Eltoukhy AA, Vegas AJ, Dorkin JR, Anderson DG. Non-viral vectors for gene-based therapy. Nat Rev Genet. 2014;15(8):541–55. https://doi.org/10.1038/nrg3763.
32. Ojea-Jimenez I, Tort O, Lorenzo J, Puntes VF. Engineered nonviral nanocarriers for intracellular gene delivery applications. Biomed Mater. 2012;7(5): 054106. https://doi.org/10.1088/1748-6041/7/5/054106.
33. Lv H, Zhang S, Wang B, Cui S, Yan J. Toxicity of cationic lipids and cationic polymers in gene delivery. J Control Release. 2006;114(1):100–9. https://doi.org/10.1016/j.jconrel.2006.04.014.
34. Bus T, Traeger A, Schubert US. The great escape: how cationic polyplexes overcome the endosomal barrier. J Mater Chem B. 2018;6(43):6904–18. https://doi.org/10.1039/c8tb00967h.
35. Knudsen KB, Northeved H, Kumar Ek P, Permin A, Gjetting T, Andresen TL, et al. In vivo toxicity of cationic micelles and liposomes. Nanomed: Nanotechnol Biol Med. 2015;11(2):467–77. https://doi.org/10.1016/j.nano.2014.08.004.
36. Barba AA, Bochicchio S, Dalmoro A, Lamberti G. Lipid delivery systems for nucleic-acid-based-drugs: from production to clinical applications. Pharmaceutics. 2019;11(8). https://doi.org/10.3390/pharmaceutics11080360.
37. Rezaee M, Oskuee RK, Nassirli H, Malaekeh-Nikouei B. Progress in the development of lipopolyplexes as efficient non-viral gene delivery systems. J Control Release. 2016;236:1–14. https://doi.org/10.1016/j.jconrel.2016.06.023.

38. Heyes J, Palmer L, Chan K, Giesbrecht C, Jeffs L, MacLachlan I. Lipid encapsulation enables the effective systemic delivery of polyplex plasmid DNA. Mol Ther. 2007;15(4):713–20. https://doi.org/10.1038/sj.mt.6300101.
39. Schafer J, Hobel S, Bakowsky U, Aigner A. Liposome-polyethylenimine complexes for enhanced DNA and siRNA delivery. Biomaterials. 2010;31(26):6892–900. https://doi.org/10.1016/j.biomaterials.2010.05.043.
40. Ewe A, Panchal O, Pinnapireddy SR, Bakowsky U, Przybylski S, Temme A, et al. Liposome-polyethylenimine complexes (DPPC-PEI lipopolyplexes) for therapeutic siRNA delivery in vivo. Nanomedicine. 2017;13(1):209–18. https://doi.org/10.1016/j.nano.2016.08.005.
41. Kwok A, Hart SL. Comparative structural and functional studies of nanoparticle formulations for DNA and siRNA delivery. Nanomedicine. 2011;7(2):210–9. https://doi.org/10.1016/j.nano.2010.07.005.
42. Pelisek J, Gaedtke L, DeRouchey J, Walker GF, Nikol S, Wagner E. Optimized lipopolyplex formulations for gene transfer to human colon carcinoma cells under in vitro conditions. J Gene Med. 2006;8(2):186–97. https://doi.org/10.1002/jgm.836.
43. Gaedtke L, Pelisek J, Lipinski KS, Wrighton CJ, Wagner E. Transcriptionally targeted nonviral gene transfer using a beta-catenin/TCF-dependent promoter in a series of different human low passage colon cancer cells. Mol Pharm. 2007;4(1):129–39. https://doi.org/10.1021/mp0600586.
44. Hanzlikova M, Soininen P, Lampela P, Mannisto PT, Raasmaja A. The role of PEI structure and size in the PEI/liposome-mediated synergism of gene transfection. Plasmid. 2009;61(1):15–21. https://doi.org/10.1016/j.plasmid.2008.08.003.
45. Opanasopit P, Paecharoenchai O, Rojanarata T, Ngawhirunpat T, Ruktanonchai U. Type and composition of surfactants mediating gene transfection of polyethylenimine-coated liposomes. Int J Nanomedicine. 2011;6:975–83. https://doi.org/10.2147/ijn.s18647.
46. Werth S, Urban-Klein B, Dai L, Höbel S, Grzelinski M, Bakowsky U, et al. A low molecular weight fraction of polyethylenimine (PEI) displays increased transfection efficiency of DNA and siRNA in fresh or lyophilized complexes. J Control Release. 2006;112(2):257–70. https://doi.org/10.1016/j.jconrel.2006.02.009.
47. Khatri N, Baradia D, Vhora I, Rathi M, Misra A. Development and characterization of siRNA lipoplexes: Effect of different lipids, in vitro evaluation in cancerous cell lines and in vivo toxicity study. AAPS PharmSciTech. 2014;15(6):1630–43. https://doi.org/10.1208/s12249-014-0193-9.
48. Khatri N, Baradia D, Vhora I, Rathi M, Misra A. cRGD grafted liposomes containing inorganic nano-precipitate complexed siRNA for intracellular delivery in cancer cells. J Control Release. 2014;182:45–57. https://doi.org/10.1016/j.jconrel.2014.03.003.
49. Safari F, Tamaddon AM, Zarghami N, Abolmali S, Akbarzadeh A. Polyelectrolyte complexes of hTERT siRNA and polyethyleneimine: effect of degree of PEG grafting on biological and cellular activity. Artif Cells Nanomed Biotechnol. 2016;44(6):1561–8. https://doi.org/10.3109/21691401.2015.1064936.
50. Upadhya A, Sangave PC. Hydrophobic and electrostatic interactions between cell penetrating peptides and plasmid DNA are important for stable non-covalent complexation and intracellular delivery. J Pept Sci. 2016;22(10):647–59. https://doi.org/10.1002/psc.2927.
51. Hu CS, Chiang CH, Hong PD, Yeh MK. Influence of charge on FITC-BSA-loaded chondroitin sulfate-chitosan nanoparticles upon cell uptake in human Caco-2 cell monolayers. Int J Nanomedicine. 2012;7:4861–72. https://doi.org/10.2147/ijn.s34770.
52. Chen CW, Yeh MK, Shiau CY, Chiang CH, Lu DW. Efficient downregulation of VEGF in retinal pigment epithelial cells by integrin ligand-labeled liposome-mediated siRNA delivery. Int J Nanomedicine. 2013;8:2613–27. https://doi.org/10.2147/ijn.s39622.
53. Xia XB, Xiong SQ, Song WT, Luo J, Wang YK, Zhou RR. Inhibition of retinal neovascularization by siRNA targeting VEGF(165). Mol Vis. 2008;14:1965–73. http://www.ncbi.nlm.nih.gov/pmc/articles/pmc2576481/.
54. Laddha AP, Kulkarni YA. Daidzein ameliorates diabetic retinopathy in experimental animals. Life Sci. 2021;265: 118779. https://doi.org/10.1016/j.lfs.2020.118779.
55. Zhang X, Bao S, Lai D, Rapkins RW, Gillies MC. Intravitreal triamcinolone acetonide inhibits breakdown of the blood-retinal barrier through differential regulation of VEGF-A and its receptors in early diabetic rat retinas. Diabetes. 2008;57(4):1026–33. https://doi.org/10.2337/db07-0982.
56. Rodriguez-Coleman H, Yuan P, Kim H, Gravlin L, Srivastava S, Csaky KG, et al. Intravitreal injection of triamcinolone for diffuse macular edema. Arch Ophthalmol. 2004;122(7):1085–6; author reply 6–8. https://doi.org/10.1001/archopht.122.7.1085.
57. Huang X, Chau Y. Enhanced delivery of siRNA to retinal ganglion cells by intravitreal lipid nanoparticles of positive charge. Mol Pharm. 2021;18(1):377–85. https://doi.org/10.1021/acs.molpharmaceut.0c00992.
58. Schmittgen TD, Livak KJ. Analyzing real-time PCR data by the comparative CT method. Nat Protoc. 2008;3(6):1101–8. https://doi.org/10.1038/nprot.2008.73.
59. Nayak K, Misra M. A review on recent drug delivery systems for posterior segment of eye. Biomed Pharmacother. 2018;107:1564–82. https://doi.org/10.1016/j.biopha.2018.08.138.
60. Bonilla L, Espina M, Severino P, Cano A, Ettcheto M, Camins A, et al. Lipid nanoparticles for the posterior eye segment. Pharmaceutics. 2021;14(1). https://doi.org/10.3390/pharmaceutics14010090.
61. Boddu SHS, Gupta H, Patel S. Drug delivery to the back of the eye following topical administration: an update on research and patenting activity. Recent Pat Drug Deliv Formul. 2014;8(1):27–36. https://doi.org/10.2174/1872211308666140130093301.
62. Gaudana R, Ananthula HK, Parenky A, Mitra AK. Ocular drug delivery. AAPS J. 2010;12(3):348–60. https://doi.org/10.1208/s12248-010-9183-3.
63. Varela-Fernandez R, Diaz-Tome V, Luaces-Rodriguez A, Conde-Penedo A, Garcia-Otero X, Luzardo-Alvarez A, et al. Drug delivery to the posterior segment of the eye: biopharmaceutic and pharmacokinetic considerations. Pharmaceutics. 2020;12(3). https://doi.org/10.3390/pharmaceutics12030269.
64. Thakur A, Fitzpatrick S, Zaman A, Kugathasan K, Muirhead B, Hortelano G, et al. Strategies for ocular siRNA delivery: potential and limitations of non-viral nanocarriers. J Biol Eng. 2012;6(1):7. https://doi.org/10.1186/1754-1611-6-7.
65. Urtti A. Challenges and obstacles of ocular pharmacokinetics and drug delivery. Adv Drug Deliv Rev. 2006;58(11):1131–5. https://doi.org/10.1016/j.addr.2006.07.027.
66. Jager RD, Aiello LP, Patel SC, Cunningham ET Jr. Risks of intravitreous injection: a comprehensive review. Retina. 2004;24(5):676–98. https://doi.org/10.1097/00006982-200410000-00002.
67. Kang-Mieler JJ, Osswald CR, Mieler WF. Advances in ocular drug delivery: emphasis on the posterior segment. Expert Opin Drug Deliv. 2014;11(10):1647–60. https://doi.org/10.1517/17425247.2014.935338.
68. Rowe-Rendleman CL, Durazo SA, Kompella UB, Rittenhouse KD, Di Polo A, Weiner AL, et al. Drug and gene delivery to the back of the eye: from bench to bedside. Invest Ophthalmol Vis Sci. 2014;55(4):2714–30. https://doi.org/10.1167/iovs.13-13707.
69. Tavakoli S, Kari OK, Turunen T, Lajunen T, Schmitt M, Lehtinen J, et al. Diffusion and protein corona formation of lipid-based nanoparticles in the vitreous humor: profiling and pharmacokinetic

considerations. Mol Pharm. 2021;18(2):699–713. https://doi.org/10.1021/acs.molpharmaceut.0c00411.
70. Sebag J. Anatomy and pathology of the vitreo-retinal interface. Eye (Lond). 1992;6(Pt 6):541–52. https://doi.org/10.1038/eye.1992.119.
71. Tavakoli S, Peynshaert K, Lajunen T, Devoldere J, Del Amo EM, Ruponen M, et al. Ocular barriers to retinal delivery of intravitreal liposomes: impact of vitreoretinal interface. J Control Release. 2020;328:952–61. https://doi.org/10.1016/j.jconrel.2020.10.028.
72. Peynshaert K, Devoldere J, De Smedt SC, Remaut K. In vitro and ex vivo models to study drug delivery barriers in the posterior segment of the eye. Adv Drug Deliv Rev. 2018;126:44–57. https://doi.org/10.1016/j.addr.2017.09.007.
73. Ruponen M, Yla-Herttuala S, Urtti A. Interactions of polymeric and liposomal gene delivery systems with extracellular glycosaminoglycans: physicochemical and transfection studies. Biochim Biophys Acta. 1999;1415(2):331–41. https://doi.org/10.1016/s0005-2736(98)00199-0.
74. Mains J, Wilson CG. The vitreous humor as a barrier to nanoparticle distribution. J Ocul Pharmacol Ther. 2013;29(2):143–50. https://doi.org/10.1089/jop.2012.0138.
75. Martens TF, Vercauteren D, Forier K, Deschout H, Remaut K, Paesen R, et al. Measuring the intravitreal mobility of nanomedicines with single-particle tracking microscopy. Nanomedicine (Lond). 2013;8(12):1955–68. https://doi.org/10.2217/nnm.12.202.
76. Xu Q, Boylan NJ, Suk JS, Wang YY, Nance EA, Yang JC, et al. Nanoparticle diffusion in, and microrheology of, the bovine vitreous ex vivo. J Control Release. 2013;167(1):76–84. https://doi.org/10.1016/j.jconrel.2013.01.018.
77. Tamboli V, Mishra GP, Mitrat AK. Polymeric vectors for ocular gene delivery. Ther Deliv. 2011;2(4):523–36. https://doi.org/10.4155/tde.11.20.
78. Liu P, Chen G, Zhang J. A review of liposomes as a drug delivery system: current status of approved products, regulatory environments, and future perspectives. Molecules. 2022;27(4). https://doi.org/10.3390/molecules27041372.
79. Mukherjee A, Waters AK, Kalyan P, Achrol AS, Kesari S, Yenugonda VM. Lipid-polymer hybrid nanoparticles as a next-generation drug delivery platform: state of the art, emerging technologies, and perspectives. Int J Nanomedicine. 2019;14:1937–52. https://doi.org/10.2147/ijn.s198353.
80. Lee CH, Ni YH, Chen CC, Chou C, Chang FH. Synergistic effect of polyethylenimine and cationic liposomes in nucleic acid delivery to human cancer cells. Biochim Biophys Acta. 2003;1611(1–2):55–62. https://doi.org/10.1016/s0005-2736(03)00027-0.
81. Pinnapireddy SR, Duse L, Strehlow B, Schafer J, Bakowsky U. Composite liposome-PEI/nucleic acid lipopolyplexes for safe and efficient gene delivery and gene knockdown. Colloids Surf B Biointerfaces. 2017;158:93–101. https://doi.org/10.1016/j.colsurfb.2017.06.022.
82. Boussif O, Lezoualc'h F, Zanta MA, Mergny MD, Scherman D, Demeneix B, et al. A versatile vector for gene and oligonucleotide transfer into cells in culture and in vivo: polyethylenimine. Proc Natl Acad Sci U S A. 1995;92(16):7297–301. https://doi.org/10.1073/pnas.92.16.7297.
83. Kircheis R, Wightman L, Wagner E. Design and gene delivery activity of modified polyethylenimines. Adv Drug Deliv Rev. 2001;53(3):341–58. https://doi.org/10.1016/s0169-409x(01)00202-2.
84. Nakhaei P, Margiana R, Bokov DO, Abdelbasset WK, Jadidi Kouhbanani MA, Varma RS, et al. Liposomes: structure, biomedical applications, and stability parameters with emphasis on cholesterol. Front Bioeng Biotechnol. 2021;9: 705886. https://doi.org/10.3389/fbioe.2021.705886.
85. Woodle MC, Collins LR, Sponsler E, Kossovsky N, Papahadjopoulos D, Martin FJ. Sterically stabilized liposomes. Reduction in electrophoretic mobility but not electrostatic surface potential. Biophys J. 1992;61(4):902–10. https://doi.org/10.1016/s0006-3495(92)81897-0.
86. Meneghetti MC, Hughes AJ, Rudd TR, Nader HB, Powell AK, Yates EA, et al. Heparan sulfate and heparin interactions with proteins. J R Soc Interface. 2015;12(110):0589. https://doi.org/10.1098/rsif.2015.0589.
87. Danielsen S, Maurstad G, Stokke BT. DNA-polycation complexation and polyplex stability in the presence of competing polyanions. Biopolymers. 2005;77(2):86–97. https://doi.org/10.1002/bip.20170.
88. Song LY, Ahkong QF, Rong Q, Wang Z, Ansell S, Hope MJ, et al. Characterization of the inhibitory effect of PEG-lipid conjugates on the intracellular delivery of plasmid and antisense DNA mediated by cationic lipid liposomes. Biochim Biophys Acta. 2002;1558(1):1–13. https://doi.org/10.1016/s0005-2736(01)00399-6.
89. Chatziralli I, Loewenstein A. Intravitreal anti-vascular endothelial growth factor agents for the treatment of diabetic retinopathy: a review of the literature. Pharmaceutics. 2021;13(8). https://doi.org/10.3390/pharmaceutics13081137.
90. Jiang X, Yang L, Luo Y. Animal models of diabetic retinopathy. Curr Eye Res. 2015;40(8):761–71. https://doi.org/10.3109/02713683.2014.964415.
91. Lai AK, Lo AC. Animal models of diabetic retinopathy: summary and comparison. J Diabetes Res. 2013;2013: 106594. https://doi.org/10.1155/2013/106594.
92. Jonas JB, Kreissig I, Sofker A, Degenring RF. Intravitreal injection of triamcinolone for diffuse diabetic macular edema. Arch Ophthalmol. 2003;121(1):57–61. https://doi.org/10.1001/archopht.121.1.57.
93. Martidis A, Duker JS, Greenberg PB, Rogers AH, Puliafito CA, Reichel E, et al. Intravitreal triamcinolone for refractory diabetic macular edema. Ophthalmology. 2002;109(5):920–7. https://doi.org/10.1016/s0161-6420(02)00975-2.